GEORG-AUGUST-UNIVERSITÄT
GÖTTINGEN

Land use and cover classification using airborne MASTER and spaceborne GeoEye-1 sensors: Focus on coffee-banana agroforestry systems near Turrialba, Costa Rica.

by

Marina Martignoni

A thesis submitted in partial fulfillment for
the degree of Master of Science in
Sustainable forest and Nature management

at the
Fakultät für Forstwissenschaften und Waldökologie
Chair of Forest inventory and Remote sensing
Georg-August Universität Göettingen, Germany

~ September 2011~

Supervisor: Prof. Dr. Christoph Kleinn _____

Co-supervisor: Prof. Dr. Martin Worbes _____

Acknowledgments

None of the achievements would have been possible without the constant, supportive and inspiring guidance of my supervisor, Dr. Hans Fuchs. His attention, hard work, prompt replies and proactive nature have set an example I hope to match some day. I am deeply indebted for what I could learn and appreciate during this experience and I shall never forget his contribution for my development.

For the completion of this thesis special thanks to:
Prof. Dr. Christoph Kleinn, for the opportunity, enlightened expertise and inspiring advice

Prof. Dr. Martin Worbes, for having being an excellent teacher and correcting this thesis

Dr. Charles Staver, for the granted financial contribution and chance to work for Bioversity

GIZ, for the funding

Dr. Lutz Fehrmann and Dr. Yang Haijun, for the statistical support and guidance

MSc. Henning Aberle, for kindly translating the abstract and sincere aid

MSc. Paul Magdon, for the inspiring discussion on sampling and classification

the whole AWF department, in particular Basanti Bharad, Beckschäfer Philip, Buschmann Axel, Dockter Ulrike, Fischer Christoph, Heydecke Hendrik, Kywe Tin Zar, Malla Rajesh, Schlote Reinhard, Vega-Araya Mauricio, for the amazing availability, kindness and good advice

Sabine Schreiner, for having being a wonderful mentor and example

Prof. Dr. Niels Stange and the whole SUFONAMA team, for allowing this great experience

the truly inspiring teachers I had in the last year, especially Dr. Stergios Adamopoulos, Dr. Gehrard Büttner, Prof. Dr. Hanns Höfle, Dr. Ronald Kühne, Prof. Dr. Bo Larsen, Prof. Dr. Ralph Mitlöhner, Dr. Carsten Schröder.

Among the Costa Rican partners:
Dr. Miguel Dita, por el apoyo excepcional y disponibilidad

Dr. Pablo Siles and Dr. Oscar Bustamante, para las observaciones siempre constructivas y la ayuda incondicional en el trabajo de campo

Dr. Ana Tapia, por las ideas

MSc Nancy Chaves, por hacerme sentir como en casa y por la experiencia inolvidable!

Dr. Christian Brennez and MSc. David Brown, por la gentil ayuda y cooperativas

Ligia Quezada and Karol Araya, para la inmensa disponibilidad y asistencia

And last but not least:
mamma e Serena, per avermi insegnato la cura e l'amore

مظفر
جس کے لیے میں بہتر بننا چاہتی ہوں جس نے میرا ساتھ د یا

all the friends met in Italy, Copenhagen, Göttingen and Costa Rica, for being just so great.

I am very thankful to you all!

Table of content

List of Figures

List of Tables

List of Abbreviations

6S : Second Simulation of a Satellite Signal in the Solar Spectrum

ACORN : Atmospheric CORrection Now

ASTER : Advanced Spaceborne Thermal Emission and Reflection Radiometer

ATREM : ATmospheric REMoval

CARTA : Costa Rican Airborne Research and Technology Application

CATIE : Centro Agronómico Tropical de Investigación y Enseñanza.

CENAT : Centro Nacional de Alta Tecnología

DEM : Digital Elevation Model

DLR : Deutsches Zentrum für Luft- und Raumfahrt

DN : Digital Number

ERSDAC : Earth Remote Sensing Data Analysis Center

FAO : Food and Agriculture Organization

FLAASH : Fast Line-of-sight Atmospheric Analysis of Spectral Hypercubes

FOC : *Fusarium oxysporum* formae specialis (f.sp) *cubense*

GDEM : Global Digital Elevation Model

GIS : Geographic Information System

GIZ : Gesellschaft für Internationale Zusammenarbeit

GSD : Ground Sample Distance

ICRAF : International Centre for Research in Agroforestry

IDL : Interface Description Language

IGM : Input GeoMetry

LCCS : Land Cover Classification Scheme

LP DAAC : Land Processes Distributed Active Archive Center

LUC : Land use / cover

MASTER : MODIS / ASTER airborne simulator

MDA : Mean Decrease Accuracy

MDG : Mean Decrease Gini

ML : Maximum Likelihood

MNF : Minimum Noise Fraction

MODIS : Moderate Resolution Imaging Spectroradiometer

MODTRAN : MODerate resolution atmospheric TRANsmission

NASA : National Aeronautics and Space Administration

OSM : OpenSteetMap

PCA : Principal Component Analysis

RGB : Red Green Blue

ROI : Region Of Interest

SGL : Super Geometry Lookup

SVM : Support Vector Machine

SWIR : Short Wave InfraRed

TIR : Thermal InfraRed

ToA : Top Of Atmosphere

VNIR : Visible Near InfraRed

Physical constants

km : kilometer

m : meter

msl : meter above sea level

µW : micro Watt

sr : steradian

W : Watt

File formats

CSV : Comma Separated Values
HDF : Hierarchical Data Format
HDR : High Dynamic Range
ODS : OpenDocument Spreadsheet
SLI : Spectral LIbrary
TIF : Tagged Image Format
TXT : TeXT

Abstract

Agroforestry is an old practice. Despite the increasing attention paid in the last decades to its ecological and economical benefits, little is known so far on the actual spatial extend. One major problem for spectral identification of agroforestry systems through remote sensing is the wide range of species and structure composition. The focus of this thesis is limited to coffee-banana mixed cropping due to the work frame constrain. This is a particularly common though threatened agroforestry system in Central America, the main reasons being intensive production and specific disease spread. The objective is to find an efficient methodology for identification of coffee-banana agroforestry in the context of land use and cover (LUC) classification. The pilot study site is located near Turrialba, Costa Rica; nevertheless a further goal is to discuss the methodology for larger areas as well. Hyperspectral visible-near and short wave infrared MASTER and spaceborne high spatial resolution GeoEye-1 data will be used as basis for image processing and analysis. A number of feature selection techniques including orthogonal transformations, FLAASH atmospheric correction and classification algorithms are tested. The results show that Maximum Likelihood (ML) algorithm lead to the best LUC classification overall accuracy (77%) as compared to Gaussian Mixture and Support Vector Machine (SVM) for the selected study site. Shade coffee agroforestry systems were classified with similar degree of confidence though it was still not possible to detect with certainty the presence of bananas and plantains.

Key words: land use/cover classification, agroforestry, MASTER, Maximum Likelihood, SVM.

Zusammenfassung

Agroforstwirtschaft ist eine alte Praxis. Trotz der zunehmenden Aufmerksamkeit, die in den letzten Jahrzehnten deren ökologische und ökonomische Vorteile zuteilwurde, ist bisher wenig über die tatsächliche räumliche Verteilung bekannt. Ein großes Problem für die spektrale Identifizierung von Agroforstsystemen durch Fernerkundung ist die breite Palette der Arten und der Strukturzusammensetzung. Aufgrund des gestellten Rahmens dieser Arbeit beschränkt sich der Fokus auf Kaffee-Bananen-Mischkulturen. Diese ist ein besonders häufiges obwohl bedrohtes Agroforstsystem in Zentralamerika. Die Hauptgründe hierfür sind intensive Produktion und die Verbreitung spezifischer Krankheiten. Das Ziel ist eine effiziente Methode zur Identifizierung von Kaffee-Bananen-Agroforstwirtschaft in dem Kontext der Klassifikation von Landnutzung und Landbedeckung zu finden. Die Pilotstudie liegt in der Nähe von Turrialba, Costa Rica. Dennoch ist ein weiteres Ziel, die Methodik auch für größere Flächen zu diskutieren. Hyperspektrale MASTER und räumlich hoch aufgelöste GeoEye-1 Satellitendaten werden als Grundlage für die Bildverarbeitung und -analyse verwendet. Eine Reihe von Feature-Auswahl Techniken einschließlich orthogonaler Transformationen, FLAASH atmosphärischer Korrektur und Klassifikationsalgorithmen werden getestet. Die Ergebnisse zeigen, dass der Maximum Likelihood (ML) Algorithmus zu der besten Genauigkeit der Klassifizierung führt (77%); im Vergleich zu Gaussian Mixture und Support Vector Machine (SVM) für das ausgewählte Untersuchungsgebiet. Schatten-Kaffee-Agroforstsysteme wurden mit einem ähnlichen Grad an Vertrauen klassifiziert, obwohl es noch nicht mit Sicherheit möglich war die Anwesenheit von Bananen und Kochbananen zu ermitteln.

Stichworte: Landnutzung / -bedeckung und Klassifizierung, Agroforstwirtschaft, MASTER, Maximum Likelihood, SVM.

1 Introduction

Agroforestry is in short the integration of forestry and agriculture. A more precise definition by ICRAF [1993] regards it as *'systems and practices where woody perennials are deliberately integrated with crops or animals in the same land-management unit, either at the same time or in sequence with each other'*. Following this, agroforestry systems can occur in different forms, from shifting cultivation to complex vegetation structures [Nair, 1985]. In his definition, Nair [1993] also mentions about the usual presence of two or more plant species, the production of at least two outputs and the significant interactions among them. Whereas most studies focused on the ecological [Jose, 2009; Palma *et al.*, 2007; Tornquist *et al.*, 1999], economic [Alavalapati *et al.*, 2004; Olschewski et al., 2006; van Asten *et al.*, 2011] and social [Cole, 2010; Isaac, 2009; Dahlquist *et al.*, 2007] benefits of agroforestry systems, little is known on their actual spatial extend [Unruh and Lefebvre, 1995; Zomer *et al.,* 2009]. Some of the figures present in the literature are summarized in Table 1. The approach used by Zomer *et al.* [2009] appears to be the most comprehensive attempt to estimate global agroforestry cover. Using 1 km resolution data, they conclude that agroforestry involves 46% of all agricultural land. One highlighted problem is that agroforestry systems are difficult to classify through remote sensing because they are composed by different plant species and have different vegetation structures, which in turn leads to very different spectral reflectance values. In spite of this, their spatial importance cannot be neglected.

Mln ha	Region	Notes	Reference
8	South and South-East Asia	Homegardens	[Kumar, 2006]
45	India, Indonesia, Mali, Niger, C. America, Spain, Portugal	Different agroforestry types	[IAASTD, 2008]
45	Europe	Silvoarable land	[Reisner *et al.*, 2007]
235	USA	Alleycropping, silvo-pasture, windbreaks and riparian buffers	[Nair and Nair, 2003]
823	worldwide	Silvopasture (516 ha)+ agroforestry (307 ha)	[Nair *et al.*, 2009]
585-1215	Africa, Asia, Americas	Agrosilvopastoral +agroforestry	[Dixon, 1995]
1000	worldwide	Tree cover >10% agricultural land	[Zomer *et al.*, 2009]

Table 1: Agroforestry extend estimates found in the literature for different regions of the globe.

Due to the conceptual frame of this thesis versus the spectral complexity of agroforestry, the focus of this research is limited to coffee-banana mixed cropping systems. The main objective is to classify land use and cover (LUC) paying special attention to agroforestry. We will use imagery from MASTER, the airborne MODIS / ASTER simulator developed by NASA for calibration of the spaceborne MODIS and ASTER satellite sensors [Hook *et al.*, 2001]. In addition, a high spatial resolution GeoEye-1 satellite scene will serve as complement for calibration, validation, visual interpretation and orientation in the field. As the MASTER images have a spatial resolution of approx. 10m and 25 bands in the visible near and short wave infrared (VNIR and SWIR) spectral range of the electromagnetic solar spectrum, a second objective is to test whether a medium spatial resolution complemented with high spectral resolution imaging sensor is capable to identify agroforestry systems. In fact, whereas high spatial resolution sensors are very powerful in identifying land cover and single objects on the ground, low and medium sensors may potentially allow best inference on land use as they take into

account spectral information from a larger surface [Clevers *et al.*, 2004; Franklin and Wulder, 2002].

The pilot study site is located near Turrialba, Costa Rica. Coffee (*Coffea* spp.) and bananas (*Musa* spp.) are respectively the first and the third cash crops in the country for land use and production value [FAO, 2003]. In addition bananas and plantains represent important stable food for locals and are commonly integrated in home gardens [Montagnini, 2006; Pocasangre *et al.*, 2011]. The association of trees to small and medium scale coffee-banana farms is common, as it provides additional income to the producers, relieves the exposure of crops to pest diseases and contributes to maintain soil fertility [Lagemann and Heuveldop, 1983].

However along with these facts small and medium scale coffee-banana producers face several challenges, namely fluctuating market prices, competition and diseases which particularly affect indigenous cultivars. One dramatic example is the so called Panama disease (*Fusarium oxysporum cubense,* FOC), a fungi which spread in the first half of 20th century across Central America and swept away entire banana plantations of the 'Gros Michel' cultivar [Ploetz *et al.*, 1999 & 2009; Blomme *et al.*, 2011]. Export-oriented farms rapidly switched to banana cultivars not affected by FOC, like Cavendish. But among locals Gros Michel is still highly preferred for paid price, taste and storage quality [Pocasangre *et al.*, 2009]. As the fungi affects mainly production rather than plant survival, many small-medium scale producers maintain Gros Michel in their farms mixed with other crops in the hope of a near future eradication of the problem.

To promote conservation, profitability and development of coffee-banana agroforestry systems in Latin America, a project called "*Mejorando la producción y mercadeo de bananos en cafetales con árboles de pequeños productores*"[1] was initiated in March 2009. The project, coordinated by Bioversity International and funded by GIZ (Deutsche Gesellschaft für

1 "Improving small farm production and marketing of bananas under trees".

Internationale Zusammenarbeit), has study sites in Costa Rica, Honduras, Nicaragua and Peru. In the specific case of Costa Rica the partners can also benefit from the facilities and support of CATIE (Centro Agronómico Tropical de Investigación y Enseñanza) research centre.

Within this international project the Chair of Forest Inventory and Remote Sensing, University of Göttingen was contacted with the goal of mapping FOC distribution in the 4 study sites. As small contribution, this thesis aims at delineating an efficient methodology to identify coffee-banana agroforestry systems using available remotely sensed images. Though this has to be considered just a pilot study, we hope that the blazed trails will serve as backbone and inspiration for further study developments in land cover and FOC mapping.

In detail the objectives of this thesis are:

- Find an effective methodology for agroforestry and LUC classification for the study site around Turrialba with the given resources;
- test the suitability of a MASTER scene at 10 m spatial resolution and 25 visible-near infrared (VNIR) and short wave infrared (SWIR) spectral bands to classify agroforestry and other land uses;
- develop a simple and concise protocol for field data collection of reference areas;
- profiling an applicable classification scheme and legend;
- evaluate the accuracy and handiness of several unsupervised and supervised classification algorithms (namely Gaussian Mixture, Maximum Likelihood and Support Vector Machine) in the context of this study;
- evaluate the advantage of atmospheric correction and feature selection for the purpose of classification.

2 Study site

2.1 Location

The study area is located in the central highlands of Costa Rica, approximately 50 km East of San José (Fig. 3 on page 10). The frame of 7 x 7 km includes the city of Turrialba and the research institute of CATIE.

2.2 Climate

The annual precipitation in Turrialba is about 2600 mm, prevalently concentrated between June and December. March is the driest month with <100 mm rainfall. Precipitation usually exceeds evapotranspiration and relative humidity is above 85% throughout the year. The mean annual temperature is 21.5°C with limited excursion [Kass *et al.*, 1995; FAOCLIM data from Fuchs *et al.*, 2010]. Because of these characteristics the area is classified in the Köppen-Geiger eco-climate scale as equatorial rainforest, fully humid [updated version for the second half of 20th century by Kottek *et al.*, 2006]. Like in other parts of Costa Rica, movements of air masses are influenced by land topography, which is briefly outlined below.

2.3 Geomorphology

The geological origin of Costa Rica is rather recent, being until 3 millions years ago just a volcanic archipelago [Coates *et al.*, 1992]. Specifically, the Turrialba valley was formed by the Rio Reventazón which eroded the substrate formed by the volcanoes Turrialba and Irazú [Kass *et al.,*1995]. The predominant soil types are Eutric Cambisol and Umbric Andosol[2] (from alluvial and volcanic origin respectively). Both substrates are

2 Nomenclature according to the World Reference Base for Soil Resources [FAO, 2006]. In soil taxonomy they are called Andic Eutropept and Acrudoxic Melanudand respectively. Eutric Cambisol is very deep, moderately well to well drained dark brown gravelly clay loam with larger stones in the subsoil. Umbric Andosol is very deep, well drained dark brown clay soil, usually located on slopes >25%. The thick A and BC layers are influenced by volcanic ashes and are highly acidic.

fertile and can be cropped easily with small addition of P and N. Lime is sometimes required for Andosols [Kass *et al.*,1995].

The study site altitude lays between 475 msl and 1225 msl, with an average of 768 msl (data obtained from DEM, chapter 3.4). Slopes are pronounced in some areas, though the average inclination is just 11˚ (20%).

2.4 Land use

The area has a good range of land cover types, which span from urban areas to forest. Agriculture is the leading activity and this provides several examples of cropping land use for spectral detection.

Little to none original vegetation is left due to slash and burn activities practiced since 3000 years. Maize, cultivated under shifting rotation, constituted the staple crop of indigenous populations; wheat, sugar cane, plantains and cattle were introduced after the Spanish reached Cartago in 1563. In the 19th century coffee became the dominant crop and, together with sugar cane, is still at the top of Turrialba agricultural production [Kass *et al.*,1995].

Coffee is usually grown under shade trees like laurel (*Cordia alliodora*) and/or poró (*Erythrina poeppigiana*) and mixed with *Musa* spp.. Laurel is native to Costa Rica and its wood is highly appreciated on the market [Butterfield and Mariano, 1995]. Poró has been introduced in the 19th-20th century from South America and is mainly used to supplement nitrogen fixation in the soil [Russo and Budowski, 1986]. These mixed agroforestry systems are reported in Costa Rica since the early 20th century [Cook, 1901], although we would like to stress the fact that agroforestry system as defined above are virtually impossible to date precisely back in time [Miller and Nair, 2006].

3 Material

3.1 MASTER images

3.1.1 Instrument and data description

The data used in this study to perform the LUC classification were acquired by the MASTER imaging sensor (Fig. 1). MASTER is the MODIS/ASTER airborne simulator developed from the joint effort of the NASA Ames Research Center, the Jet Propulsion Laboratory and the EROS Data Center. The main objectives of this cooperation were the elaboration of algorithms, calibration and validation of data for MODIS[3] and ASTER[4], spaceborne sensors flying on the Terra platform [NASA, 2008].

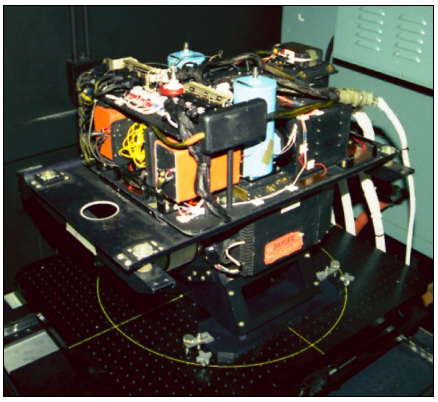

Fig. 1: MASTER camera. Image from http://asapdata.arc.nasa.gov/Image.htm. A full description of the optical and electronic systems is provided by Hook *et al.* [2001].

MASTER scanning radiometer records radiance data in 50 spectral bands[5], from the VNIR (visible near infrared) to the TIR (thermal infrared) regions of the electromagnetic spectrum (Table 2). The channel position has been designed to simulate at best both ASTER and MODIS measurements (Fig. 2). The ground spatial resolution depends on the terrain surface and on the flying altitude of the aircraft. For MASTER it normally lies between 5 and 50 m (Table 3).

3 MODIS: Moderate Resolution Imaging Spectroradiometer.

4 ASTER: Advanced Spaceborne Thermal Emission and Reflection Radiometer.

5 Stored at 16-bits resolution.

Channel	Full width half maximum	Channel center	Channel peak	Channel	Full width half maximum	Channel center	Channel peak
1	0.0433	0.4574	0.458	26	0.1559	3.1477	3.142
2	0.0426	0.4981	0.496	27	0.1459	3.2992	3.292
3	0.0427	0.54	0.538	28	0.1478	3.4538	3.452
4	0.0407	0.5807	0.58	29	0.1544	3.6088	3.607
5	0.0585	0.6599	0.652	30	0.1345	3.7507	3.757
6	0.042	0.711	0.71	31	0.1524	3.9134	3.912
7	0.0418	0.7499	0.75	32	0.1548	4.0677	4.067
8	0.042	0.8	0.8	33	0.153	4.2286	4.224
9	0.0417	0.8658	0.866	34	0.153	4.3786	4.374
10	0.0407	0.9057	0.906	35	0.1446	4.5202	4.522
11	0.0403	0.9452	0.946	36	0.1608	4.6684	4.667
12	0.0542	1.6092	1.608	37	0.1521	4.8233	4.822
13	0.0526	1.6645	1.666	38	0.1487	4.9672	4.962
14	0.0514	1.7196	1.718	39	0.1495	5.116	5.117
15	0.0521	1.7748	1.774	40	0.1578	5.2629	5.272
16	0.0506	1.8281	1.826	41	0.3645	7.7599	7.815
17	0.0457	1.8751	1.874	42	0.4333	8.1677	8.185
18	0.0575	1.9244	1.924	43	0.3543	8.6324	8.665
19	0.0504	1.9807	1.98	44	0.4253	9.0944	9.104
20	0.0481	2.0806	2.08	45	0.4083	9.7004	9.706
21	0.0511	2.1599	2.16	46	0.3963	10.116	10.115
22	0.0508	2.2106	2.212	47	0.5903	10.6331	10.554
23	0.0513	2.2581	2.258	48	0.6518	11.3293	11.365
24	0.0683	2.3284	2.32	49	0.4929	12.117	12.097
25	0.0641	2.3939	2.388	50	0.4618	12.8779	12.876

Table 2: Spectral characteristics of MASTER channels. On the left (channels 1-25): VNIR and short-wavelength infrared (SWIR) band definition. On the right (channel 26-50): mid-thermal infrared (mid-TIR). Table from Hook *et al.*[2001].

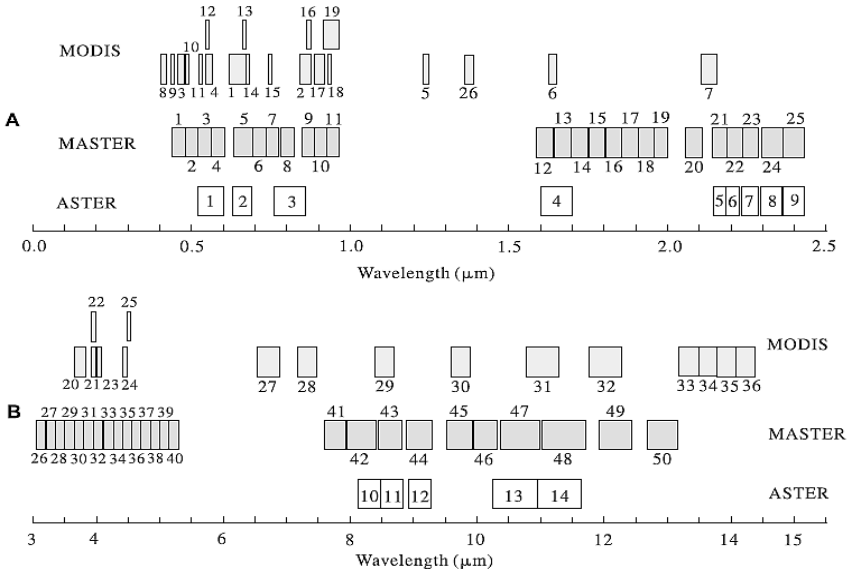

Fig. 2: Channels and wavelength regions of the MODIS, ASTER and MASTER radiometers. (a) reflective channels, (b) thermal channels. Boxes represent the bandwidth for each sensor channel. The numbers refer to the band numbers for each sensor. Image from Li and Moon [2004].

A full description of MASTER optical and electronic devices is given by Hook *et al.* [2001]. They also provide specific information about in-flight calibration depending on the utilized aircraft platform. Spectral and radiometric calibration of channels is performed on a regular basis pre- and postflight (see Arnold *et al.* [1996] for procedure details).

Wavelength range	0.4–13 μm
Number of channels	50
Number of pixels	716
Instantaneous field of view	2.5 mrad
Total field of view	85.92°
Platforms	DOE King Air Beachcraft B200, NASA ER-2, and NASA DC-8
Pixel size DC-8	10–30 m
Pixel size ER-2	50 m
Pixel size B200	5–25 m
ER-2 range (without refueling)	3700 statute miles
B200 range (without refueling)	700 statute miles
DC-8 range (without refueling)	5403 statute miles
Scan speeds	6.25/12.5/25 rps
Products	Radiance at sensor (Level 1B)
Calibration VIS-SWIR	Laboratory Integrating Sphere
Calibration MIR-TIR	2 on-board blackbodies
Data Format	Hierarchical Data Format (HDF)
Digitization	16-bit

Table 3: Summary of MASTER sensor characteristics. B200, DC-8 and ER-2 refer to different aircraft models used by NASA. Table from Hook *et al.* [2001].

Examples for MASTER data can be ordered free of charge from the NASA Jet Propulsion Laboratory website <http://masterweb.jpl.nasa.gov/>, at a maximum of 5 scenes per order. They are compiled as Level-1B product, which means that data are already available in radiance-at-sensor values and contain ancillary information about geo-location, navigation and calibration [Eurimage, 2011]. MASTER data are stored in the Hierarchical Data Format (HDF4).

3.1.2 CARTA mission

Costa Rican Airborne Research and Technology Applications (CARTA) missions are a cooperation between the Centro Nacional de Alta Tecnologia (CENAT) and NASA. The main objectives are the acquisition of airborne images of Costa Rica for national use and scientific research. Until now there have been two CARTA missions, one in 2003 and one in 2005. In both these occasions four sensors have been used to collect digital scanner data and and analogue airphotos: MASTER airborne simulator, Leica RC-30 metric camera, Cirrus Digital Camera System (DCS) and HyMap hyperspectral scanner [ISDA, 2011]. These information about the CARTA mission are provided here as

context background and as sparkle for further sensor comparison studies.

The selected MASTER image for this research was taken on March 11th during the CARTA 2005 mission (tile code: MASTERL1B_0500311_04_20050307_1516_1543_V01) (Fig. 3). As the study site was fully covered by this scene and without cloud cover it was not necessary to mosaic several tiles. The High Altitude WB-57 aircraft used flew at 8438-8459[6] m height allowing a 10 m spatial resolution on the ground.

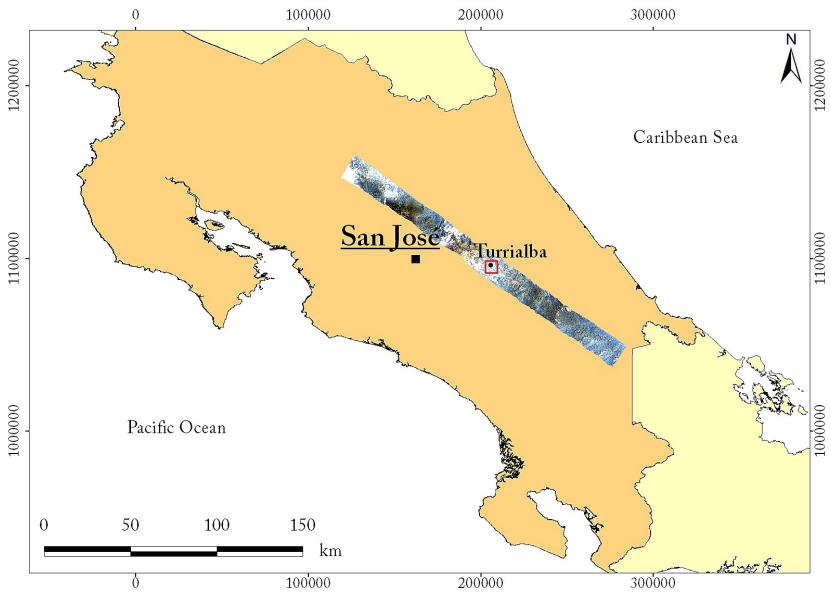

Fig. 3: Study site indicated by the red frame (7× 7 km) around the city of Turrialba, Costa Rica. The MASTER tile (MASTERL1B_0500311_04_20050307_1516_1543_V01) from March 11th, 2005 was georectified using ENVI. Tile swath width: 14.2 km; scanline length: 200 km. Grid projection system: UTM Zone 17N, Datum: WGS-84. Map produced in ArcMap 10.0.

Seasonal phenological variation can be a problem for remote sensing LUC classification, especially when focusing on natural environments. The selected MASTER scene was taken in March, the driest month of the year, which lowers the chances of cloud and haze presence but could also mean lower vegetation cover. Thus, although for LUC

6 Data measured with a GPS device on the aircraft and retrieved from the MASTER Header File.

visual interpretation we do not expect major problems as rarely evapotranspiration > precipitation for a period long enough for plants to dry out in a tropical rainforest region [Eva *et al.*, 2004], some underestimations of vegetation cover should be accounted.

3.2 GeoEye-1 images

GeoEye-1 images were used to complement LUC visual interpretation and facilitate orientation in the field. GeoEye-1 is a satellite launched in orbit on September 8th, 2008 by GeoEye. It is designed and equipped with very advanced technology which allows the highest resolution among commercial satellites. It records spectral data in one panchromatic band (ground sampling distance, GSD=0.41m[7]), one near infrared and three visual RGB bands (GSD=1.65m).

The study site around Turrialba belongs to a scene acquired on February 5th, 2010 (order identifier: 20100205_16072001603031604257). This image is available for private and unpublished works without concession through the GoogleEarth™ platform, as long as any reproduction carries the disclaimer attributes. Alternatively the raw image in 5 bands can be purchased through the GeoEye website (http://www.geoeye.com : GeoFuse → Advanced search → Upload file → Open Permalink).

As the purposes of this thesis did not involve any GeoEye image analysis, simple screen-shots were taken from GoogleEarth. Only at the very end a standard product covering the considered study site was ordered for evaluation and further research developments within the funding project.

To facilitate LUC classification a raster file was created based on the GeoEye image. 432 screen-shots were taken from 1.15 km zenith distance from the ground and mosaiced using Photoshop CS4. This mosaic was then manually georeferenced in Quantum GIS.

7 Rounded to 0.5 m due to US Government restrictions on civilian imaging.

3.3 OpenStreetMap

OpenStreetMap (OSM) is an open source, geospatial project where geographic data are collected and shared. The aim is to create freely editable and accessible maps of the whole world licensed under the Creative Common Attribution-ShareAlike 2.0. This means that it is possible for example to download spatial references such as street maps which have been traced with *in situ* GPS records without the burden of legal or technical restrictions. A very handy plug-in allows to invoke and download target OSM layers directly from the QuantumGIS working project. The OSM layers are considered to have generally a good degree of spatial accuracy [Haklay and Weber, 2008; Mooney *et al.*, 2010].

3.4 Digital elevation model

A digital elevation model (DEM) of Costa Rica with 30 m spatial resolution was available and used to retrieve basic information such as elevation and slope when not directly possible from the MASTER image. This DEM was produced from the ASTER scene archive during the ASTER Global DEM (GDEM) mission [ASTER GDEM validation team, 2009]. The GDEMs are available for download from the Earth Remote Sensing Data Analysis Center (ERSDAC) of Japan or the NASA's Land Processes Distributed Active Archive Center (LP DAAC) websites.

3.5 Software programs

To perform the study the following software programs were used:

Licensed	**Open source**
• Adobe Photoshop CS4	• DNRGarmin 5.4.1
• ESRI ArcGIS Desktop 10.0	• EnMAP Box 1.1 (64-bit operating systems)
• ITT ENVI 4.8	• JabRef 2.6
	• OpenOffice 3.1
	• QuantumGIS 1.7
	• R 2.13

4 Land use and cover (LUC) classes

The LUC classes used in this study are a modified version of the FAO[8] land cover classification systems (LCCSs) and IGBP[9] legend. The applied modifications mainly aim at reducing the number of classes while highlighting the prominent land features of the study area. Before proceeding with describing the classes used, it is important to clarify the meaning of the following terms:

Land cover: "the bio-physical cover on the Earth surface" [Di Gregorio and Jansen, 1998]. E.g.: tree, mixed shrub-tree stand, water body, bare soil.

Land use: "the arrangements, activities and inputs people undertake in a certain land cover type to produce, change or maintain it" [Di Gregorio and Jansen, 1998]. E.g.: tree plantation, agroforestry system, swimming pool, pit.

Legend: the list of classes resulting from the classification of a specific area, using a defined mapping scale and data set [Di Gregorio and Jansen, 1998]. All classes should be mutually exclusive[10] and total exhaustive[11] [Congalton, 1991]. Both the FAO and IGPB use discrete classes to arrange continuous variables (such as vegetation cover) in nominal scale [Di Gregorio and Jansen, 1998], which are suitable for discussion and comparison. There are however also examples of legend based on continuous gradients such as the MODIS Vegetation Continuous Fields (VCF) or AVHRR CF datasets [Schwarz and Zimmermann, 2005; Zomer *et al.*, 2009], which are arguably closer to reality but can be

8 FAO: Food and Agriculture Organization.

9 IGBP: International Geosphere-Biosphere Programme. Their land cover legend and map [Loveland *et al.*, 2000] are one of the eight used for the Global Land Cover Characteristics (GLCC) database generated by the U.S. Geological Survey's (USGS) National Center for Earth Resources Observation and Science (EROS), the University of Nebraska-Lincoln (UNL) and the Joint Research Center of the European Commission.

10 Each pixel should be classified unambiguously as belonging either to one or to the other class.

11 All pixels of the study area should fall into one of the classes.

applied only to few LUC classes at a time. The mapping legend used by the FAO Forestry department [FRA, 2010] is presented in Appendix A.

Classification: abstract representation of the reality as resulting from diagnostic criteria. It describes both the discerning rules used by the classifier and the associated outputs. A classification scheme can be *hierarchical* or *non-hierarchical* [Di Gregorio and Jansen, 1998]. As the term explains, in the former the classes are assigned with progressively level of detail, whereas in the latter all classes are defined at once. The FAO LCCS is an example of hierarchical classification (Fig. 4), while the IGBP legend is non-hierarchically defined (Fig. 5).

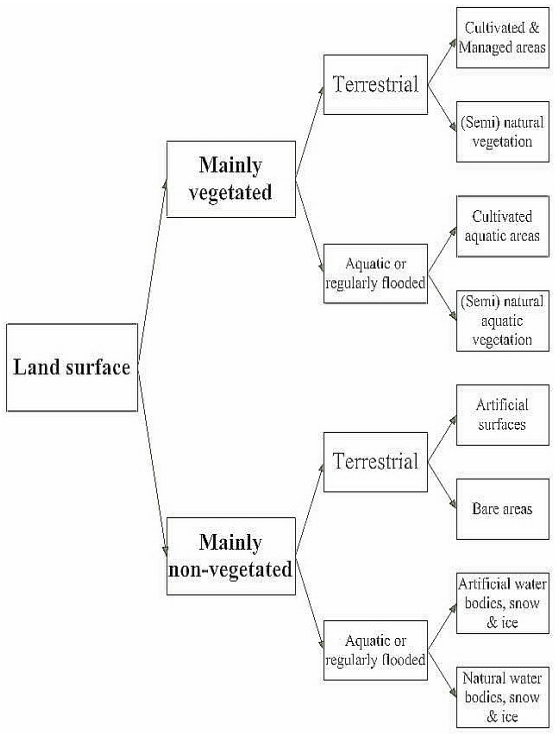

Fig. 4: LCCS used by the FAO. The scheme resembles the hierarchical order. The resulting legend depends on the accomplished detail level [DiGregorio &Jansen,1998]

CLASS	CLASS NAME	DESCRIPTION
1	Evergreen Needleleaf Forests	Lands dominated by trees with a percent canopy cover >60% and height exceeding 2 meters. Almost all trees remain green all year. Canopy is never without green foliage.
2	Evergreen Broadleaf Forests	Lands dominated by trees with a percent canopy cover >60% and height exceeding 2 meters. Almost all trees remain green all year. Canopy is never without green foliage.
3	Deciduous Needleleaf Forests	Lands dominated by trees with a percent canopy cover >60% and height exceeding 2 meters. Consists of seasonal needleleaf tree communities with an annual cycle of leaf-on and leaf-off periods.
4	Deciduous Broadleaf Forests	Lands dominated by trees with a percent canopy cover >60% and height exceeding 2 meters. Consists of seasonal broadleaf tree communities with an annual cycle of leaf-on and leaf-off periods.
5	Mixed Forests	Lands dominated by trees with a percent canopy cover >60% and height exceeding 2 meters. Consists of tree communities with interspersed mixtures or mosaics of the other four forest cover types. None of the forest types exceeds 60% of landscape.
6	Closed Shrublands	Lands with woody vegetation less than 2 meters tall and with shrub canopy cover is >60%. The shrub foliage can be either evergreen or deciduous.
7	Open Shrublands	Lands with woody vegetation less than 2 meters tall and with shrub canopy cover is between 10-60%. The shrub foliage can be either evergreen or deciduous.
8	Woody Savannas	Lands with herbaceous and other understorey systems, and with forest canopy cover between 30-60%.The forest cover height exceeds 2 meters.
9	Savannas	Lands with herbaceous and other understorey systems, and with forest canopy cover between 10-30%.The forest cover height exceeds 2 meters.
10	Grasslands	Lands with herbaceous types of cover. Tree and shrub cover is less than 10%.
11	Permanent Wetlands	Lands with a permanent mixture of water and herbaceous or woody vegetation that cover extensive areas. The vegetation can be present in either salt, brackish, or fresh water.
12	Cropland	Lands covered with temporary crops followed by harvest and a bare soil period (e.g., single and multiple cropping systems. Note that perennial woody crops will be classified as the appropriate forest or shrub land cover type.
13	Urban and Built-up	Land covered by buildings and other man-made structures. Note that this class will not be mapped from the AVHRR imagery but will be developed from the populated places layer that is part of the Digital Chart of the World.
14	Cropland/Natural Vegetation Mosaics	Lands with a mosaic of croplands, forest, shrublands, and grasslands in which no one component comprises more than 60% of the landscape.
15	Snow and Ice	Lands under snow and/or ice cover throughout the year.
16	Barren	Lands exposed soil, sand, rocks, or snow and never has more than 10% vegetated cover during any time of the year.
17	Water Bodies	Oceans, seas, lakes, reservoirs, and rivers. Can be either fresh or salt water bodies

Fig. 5: Legend used in the IGBP LCCS. The classes are non-hierarchically defined [FRA, 2000a].

Now that the terms land cover/use became familiar and these two officially recognized classification schemes were briefly introduced, it is possible to speculate that the FAO distinction between 'cultivated/managed areas' and 'natural vegetation' or the IGPB definition of 'cropland' do involve some sort of land use knowledge. However, far from debating here this choice, in this thesis we will keep on referring to their schemes as LCCS. We prefer anyway to include the term 'use' for our classification scheme and legend.

Because of the objectives and smaller scale of this study, the global scale FAO and IGBP LCCSs had to be reduced or slightly modified. The principles to design the LUC classification scheme were:

- adhere as much as possible to the FAO and IGBP LCCSs;

- be hierarchical, in order to be easily implemented in Decision Trees[12] and larger areas.

We wanted the resulting legend to be:

- applicable at the given spatial resolution;

- meaningful to fulfill the objectives (thus irrelevant classes excluded);

- site adapted (thus unobserved classes excluded).

A visual representation of the adopted classification scheme and legend are presented in Fig. 6 and Table 4.

The distinction between tree/shrub/herbaceous life forms follows a simplified version of Raunkiær's classification (Appendix B). The aim was to shape artificial class delineations in a way that better resembles natural breaks. The class threshold values are inspired either by the FAO Forest Resource Assessment report [FRA, 2010] or by the IGBP definitions, depending on the context and objectives. Agricultural land is separated from non-agricultural land on the basis of produced good (crop vs. wood respectively) [FRA 2000b].

12 Decision Trees are a branch of classification algorithms based on the mapping of decision rules and relative outputs in a tree-like format, normally dichotomous.

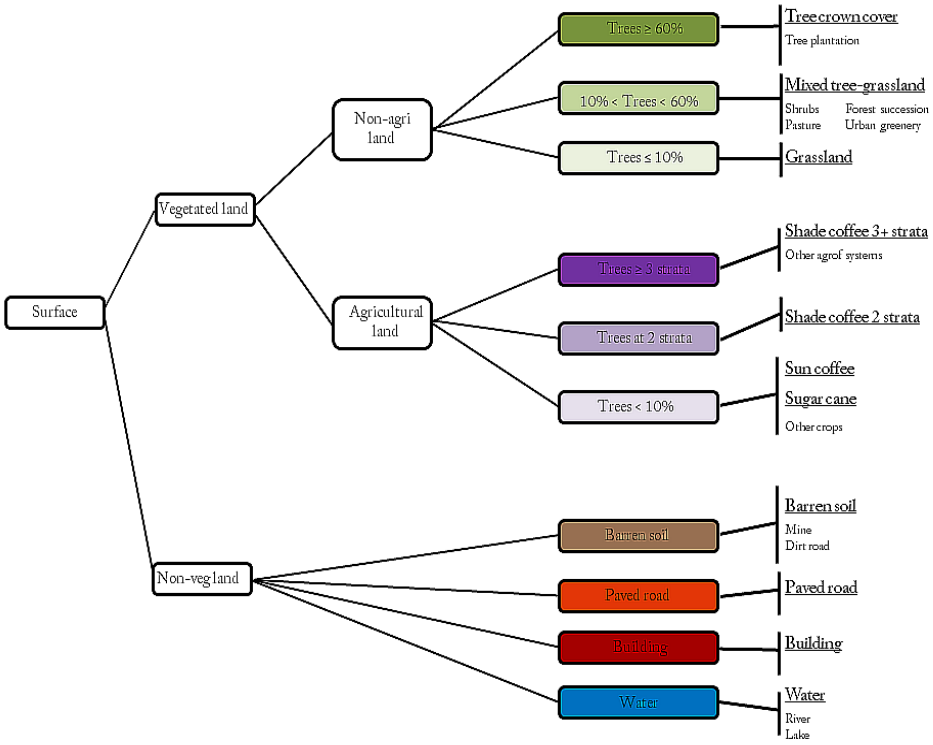

Fig. 6: LUC classification scheme applied in this study. The underlined LUC class names on the right are those selected for the final legend; the others written in smaller font are just possible LUC classes not found or not applied in this study. 'Vegetated land' is defined as land with ≥10 % vegetation cover [FRA, 2000b]. 'Agricultural land' is defined on the basis of produced crop type and excludes tree plantations [FRA, 2000a]. Other thresholds are taken from the FAO or from the IGBP LCCSs [FRA, 2010].

According to the FAO [FRA, 2010] agroforestry systems are classified as 'Other land' (more precisely as sub-category 'Other land with tree cover' given that trees are >10%). Note that coffee agroforestry systems might or might not be associated with trees and still be classified as such, as the coffee bushes themselves are occasionally used as woody fuel [Thacher *et al.*, 1996]. Although more speculations on tree cover thresholds in agroforestry can be discussed [Zomer *et al.*, 2009], the agroforestry systems observed in the region were only shade coffee plantations, thus implying a degree of tree cover (tree plants are estimated to cover approx. 50% of land according to a previous work by

Lichtemberg [2010] on agroforestry systems at ≥3 strata in the same region)[13].

No.	ID	Color	Class name	Definition
1			Tree crown cover	Non-agricultural area >60% covered by the nadir tree crown projection on the ground.
2			Shade coffee at ≥3 strata	Coffee shrubs grown under trees with ≥3 strata vegetation structure.
3			Shade coffee at 2 strata	Coffee shrubs grown under trees with 2 strata vegetation structure.
4			Sun coffee	Sun-grown coffee plantation.
5			Sugar cane	Sugar cane plantation.
6			Mixed tree-grassland	Non-agricultural land covered with herbaceous species and 10%≤tree cover≤60%.
7			Grassland	Non-agricultural land covered with herbaceous species and <10% tree cover.
8			Bare soil	Land with <10% vegetation cover and exposed soil, sand or rocks.
9			Paved road	Roads covered with asphalt.
10			Building	Buildings or other similar man-made structures.
11			Water bodies	Visible surface water.

Table 4: Legend of land use and cover (LUC) classes applied to classify the MASTER image over the study site of 7 × 7 km near Turrialba (Costa Rica) at a spatial resolution of 10 m. Agricultural land is defined on the basis of produced crop type and excludes tree plantations [FAO, 2000b]. Other thresholds are taken from the FAO or from the IGBP LCCSs [FRA, 2010].

13 Silvopastoral systems are included in the class 'mixed tree-grassland'. Although they are agroforestry systems they are not considered in a separate class in this thesis due to the spectral similarity with, for example, urban greenery.

Musa spp. are often integrated in these shade coffee cropping systems. However, due to the reduced sample size and resolution of the MASTER scene it was not possible to infer on the presence or absence of banana and plantains in shade coffee plantations only from remote sensing. Thus we will limit the agroforestry class definition to shade coffee at 2 or at more vegetation strata, implying that in a 2 strata agroforestry systems there are usually 2 species (coffee and one tree species) whereas in a system at ≥3 strata they are usually more (coffee and several tree species and/or *Musa* spp.).

Cloud and shadow classes are absent in the legend. This was clear from simple visual inspection of the MASTER image, though the decision became definitive after evaluating the results of preliminary unsupervised classifications.

Burned land (usually sugar cane fields) could also not be detected from visual inspection of the MASTER and GeoEye-1 images, even if likely present on the ground. Other potential land use classes (e.g. mixed shrubs-grassland, forest clear cuts) were excluded as no matching data were observed.

A draft of LUC classification was drawn before going to the field, though the most suitable classes were delineated only after data collection. The FAO [Di Gregorio *et al.,* 1998] regards this classification scheme as *a posteriori* approach, like the Braun-Blanquet system. The disadvantages of this approach are the limited application scale of the legend on wider landscapes, site-specificity and the risk of incurring in ambiguous field notes. However for the identification of agroforestry systems in the selected area and of specific land use types not recognizable from the MASTER image, *a posteriori* classification proved to be the most suitable. For example distinction between 'cropping land with trees at 2' and 'at ≥3 strata' could be defined only during data collection.

5 Methodology

In this chapter the methodological theory applied to process and classify the MASTER image is outlined. When needed, more technical references on the procedures are available in the appendices.

5.1 Sampling design

When performing any classification with remote sensed resources, it is indispensable to ensure references for the output accuracy. The references can be already validated thematic maps, interpreted space- or airborne images, ground truth collection or a combination of both [Plourde and Congalton, 2003; Stehman and Czaplewski, 1998]. In this study we opted for a visual interpretation of the MASTER and GeoEye-1 image accompanied by field data collection. The choice of the population size and sampling design was conceived to be as efficient as possible in terms of logistic, time and financial resources. At the same time the aim was to maintain a scientifically sound and statistically valid approach.

The sampling design is the protocol adopted to select the observation units [Stehman and Czaplewski, 1998]. As the majority of land use and forest inventories, the applied sampling technique in this study is systematic sampling. This means that the location of the observation plots follows a systematic pattern [Kleinn, 2007]. Drafting a sampling protocol requires delineations of the population, sampling frame, sampling plot and sampling unit, hereinafter defined.

5.1.1 Population

As mentioned in 2.1, a study area of 7 x 7 km has been selected. Having a spatial resolution of 10 m, it is equivalent to about 490 000 pixels. This can be considered our population, better defined as the the interest domain of the study [Kleinn, 2007].

5.1.2 Sampling frame

The sampling frame delimits and identifies the *sample* population [Stehman and Czaplewski, 1998]. In the case of a map, a sampling frame can be areal boundaries which include all the sampling plots.

The question on how large should the sample population be in order to fulfill a certain accuracy confidence interval does not have an easy answer. This is why a summarized literature review on the topic is introduced before presenting the chosen sample size for this study.

Short literature review on sample size for remote sensed data

The following selections are mainly based on Foody *et al.* [2006], Tso and Mather [2009], and Van Genderen *et al.* [1978]. It emerges that:

- the sampled data must adequately represent the temporal state of the observed phenomena, especially if the target classes are of a temporally changing nature [Tso and Mather, 2009];
- several authors [Atkinson, 1996; Curran, 1988; Van der Meer *et al.*, 1999; Wang *et al.* 2005; Woodcock *et al.*, 1988] recommend the use of geostatistical methods to choose the most appropriate sampling scheme in remote sensing because since sampling sites have fixed locations in space their attributes are correlated and must therefore be handled differently than standard statistical rules;
- sample size is related to the observation scale, as the scale determines the sampling units and thus the variability within them. For being adequate the sample size should account for variance between classes [Tso and Mather, 2009];
- researchers dealing with multi- and hyperspectral data should bear in mind that the higher the number of features, the larger sample size should be in order to maintain same accuracy degree (Hughes phenomenon [Hughes, 1968]);
- Mather [2004] advises to equal the minimum sample size per each class to the

number of features multiplied by 30. He bases this figure on the notion that in univariate statistics a sample size >30 is considered large;

- Congalton [1991] experienced that 50 is a reasonable sample size for each vegetation class (increased to 75-100 if the area is >1 mln acres or considering >12 classes);
- Van Genderen *et al.* [1978] propose some tables in their article to estimate the required sample size depending on different confidence probabilities: for example 20 and 30 should be respectively the class sample size for 85% and 90% accuracy.
- Congalton and Green [1999] propose a formula to estimate the minimum sample size for specific confidence intervals that reflects the class multinomial distributions[14];
- another possible approach is to base the decision on the class variance with $n=t^2s^2/A^2$ where n is the sample size, t is the t-distribution, s is the standard error and A is the confidence interval width [Foody *et al.*, 2006; Kleinn, 2007]. This is in line with the consideration that the model of data distribution is crucial: for example a classifier such as Maximum Likelihood (5.4.2) requires values for the mean vector and the variance-covariance matrix per each class to operate effectively [Tso and Mather, 2009];
- other statistic formulas accounting for the data distribution are discussed by Fitzpatrick-Lins [1981] and Congalton [1991];
- generalizing this concept, Foody *et al.* [2006] state that the for supervised classification the training set size is not fixed but can vary considerably depending on the properties of the chosen classification algorithm[15];
- the estimations mentioned above might be severely influenced by erroneous or unrepresentative samples included in the training set. Though the effect of

14 $n = B\Pi_i(1 - \Pi_i) / b_i^2$ where: n is the sample size; B the upper $(\alpha/k) \times 100^{th}$ percentile of the chi-square distribution; α the required confidence lever; k the number of classes; Π_i the percentage of land covered by class i; and b the required precision in percentage.

outliers should be limited for large samples, Mather [2004] presents a supportive method to weight the observations.

Applied sample size

In spite of all these considerations, usually costs, access to sampling sites and resource availability constrain data collection. In addition in our case no estimations on land use could be exploited prior the actual data collection. Thus, being a pilot study, it is acceptable to base the decision of the sample size simply on the objectives and context constrains, postponing the evaluation of sample size adequacy to the Discussion and Outlooks chapters.

The sampling plots were distributed into 36 quadrants, each of 200 × 200 m (4 ha) and all the surface within these quadrants was scheduled to be surveyed. The above seemed in fact reasonable figures to cover the highest number (possibly all) land use types and limit time and travel costs.

The systematic sampling frame was drawn as follows:

- overlay of a square grid of quadrants to the 7 x 7 km study site using a geographical information system (GIS) software. Quadrant (grid cell) size: 200 x 200 m. Grid orientation: North-South.
- Random selection of one quadrant by the GIS software[16].
- Systematic selecting other 35 quadrants at 1200 m distance[17].

No slope correction was applied to these quadrants since the object of interest was the number of pixels (which are our sampling units, see below) and not the surface area.

15 For example in the case of Maximum Likelihood (ML) supervised algorithm the mean vector and the variance-covariance matrix per each class necessary to perform the classification influence the sample size. For Support Vector Machine (SVM) classifier 4 very interesting strategies are proposed by Foody *et al.* [2006] for improving accuracy and reducing considerably sample size.

16 In Quantum GIS©: Vector → Research Tools → Random selection.

17 Distance between any point in a quadrant and its equivalent in the adjacent quadrant = $\sqrt{\frac{49000000}{36}} = \sqrt{1361111.1111} \approx 1200\text{m}$

5.1.3 Sampling plot and unit

Theoretically, a systematic grid should be seen as a large cluster plot made of several sub-plots [Kleinn, 2007]. Stehman and Czaplewski [1998] define sampling plots as all the sites that are actually sampled. However for simplicity in this thesis we will use the terms *quadrants* and *sampling polygons* to refer respectively to the grid sub-plots and to the actual sampling plots. Sampling polygons were digitized on-screen within each quadrant by partitioning the image into regions of homogeneous neighboring pixels. A LUC label was assigned to each polygon following the legend on page 17; by doing so all the polygon belonging pixels were also automatically labeled. For a full procedure description see Appendix C. This process called *visual interpretation* was performed by one person only using the georectified MASTER image and GeoEye-1 mosaic (Fig. 7).

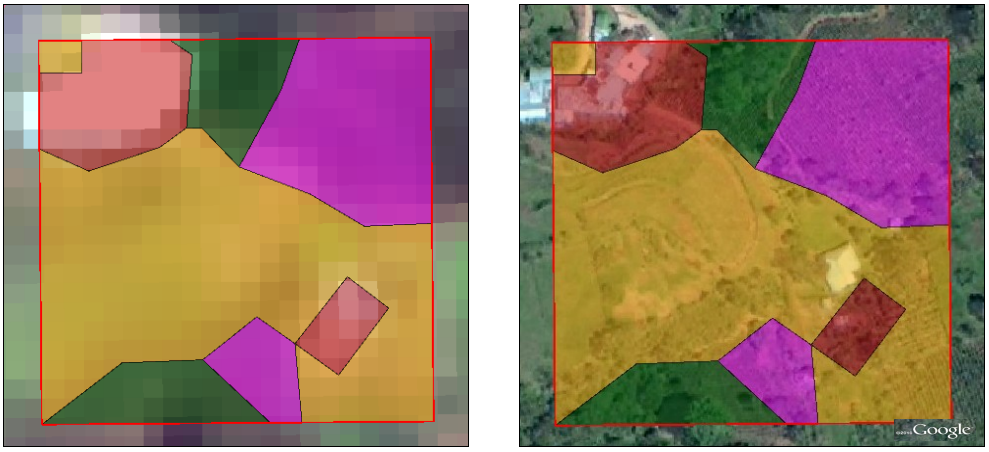

Fig. 7: Left: one of the 36 selected sampling quadrants (red frame), whose land use classes have been digitized and visually interpreted over MASTER-1B georectified product (RGB: 5;3;1). Right: the same quadrant over the GeoEye-1 mosaic. The colored polygons represent different land use classes (legend on page 17). Spatial offset is discussed in 6.3.1.

Care was taken to avoid polygon overlapping. At the end of the digitization, a vector file was created for each LUC class. The digitized polygons represent our sampling plots. Contrary, *sampling units* are defined as the reference units upon which the accuracy assessment is based [Stehman and Czaplewski, 1998]. Thus the ultimate sampling units

of this study are the image pixels and should not be confused with the sampling plots. If preferred, sampling plots can be thought as spatial pixel clusters. In order to be considered 'ground truths' the polygons need field validation [Congalton, 1991]. Due to unavoidable human error, they will be hereinafter referred to as reference areas and not exactly as ground truths.

5.2 Data collection

The response design defines the methodology to collect information on the LUC reference sites [Stehman and Czaplewski, 1998]. Though in this sub-chapter only a brief overview on the methodology is provided, a more detailed description is listed in the field manual (Appendix I).

To validate the polygon land use on the field the followed procedure involved:

- location of the quadrant(s) position using GPS device and hard/soft maps;
- identification of the virtual boundaries of the sampling polygons;
- checking the polygon shape and assigned class value;
- registration of GPS coordinates and acquisition of digital photos from the observation point, useful in case of doubt or as a record for future comparison.

Due to the broad class definition in the legend, it is possible to assess the class belonging by simple visual survey of the area. If any land use change occurred between the MASTER (2005) or the GeoEye-1 (2010) image acquisition and the field survey (2011), we attempted to trace back to the land use in 2005 and annotate the inconsistency.

To help data collection the used field form template is shown in Appendix D. Once the field data collection is concluded, it is necessary to upload the land use information and GPS points into vector layers. The digitized and field validated polygons become in this way the regions of interest (ROIs) used as reference areas for accuracy assessment and to train the supervised classifiers (chapter 5.4.2).

Data collection designed in this way can be preformed by one operator alone, though two is the recommended number. Other equipment details are present in the field manual. The average sampling speed, with the given location, resources and conditions, was 4 quadrants per day. Data collection for this study was carried out in May. This field procedure is rather economic in terms of time and money, with transportation being the main factor to be considered.

5.3 Image processing

5.3.1 Georeferencing and subsetting the image

Once received the MASTER-1B tile in HDF format it is necessary to assign precise coordinates to the image (georeferencing[18]) and subset the study area. The *ENVI tutorial: Geo-referencing images using Input Geometry* provided a suitable backbone scheme for geo-rectification, though some modifications were required (Appendix E). Note that to follow these steps platform geometry information are necessary. In case of MASTER products they are incorporated into the HDF file, specifically under the datasets 'PixelLatitude' and 'PixelLongitude'. After georeferencing, the MASTER image will be overlapped with both the GeoEye-1 mosaic manually georectified and layers from OpenStreetMap (OSM) to test the accuracy of geometric correction.

Subsetting the image was performed by overlapping the study area vector file to the georeferenced MASTER tile. Alternatively, the exact geographic extension of the study area can be used. The MASTER image was also spectrally subset, selecting only the first 25 visible-near infrared and short wave infrared (VNIR-SWIR) bands and excluding the remaining 25 thermal infrared (TIR) ones. This choice was driven by the preference of reducing data size and by the lower spatial resolution of TIR channels [Gelli and Poggi, 1999; Tso and Mather, 2009]. In addition TIR bands requires different calibration methodologies and handling, as they record emissivity and not reflectance.

18 In this thesis the terms georeferencing and georectification will be used interchangeably.

5.3.2 Atmospheric correction

As indicated in Table 3, MASTER-1B products are already dispatched as 'radiance-at-sensor' values; this means that digital numbers (DNs) have already been translated into radiance values using the offset and gain metadata of instrument calibration. *Radiance* is the radiant energy emitted from a particular area per unit time at a given solid angle in a specified direction [Jensen, 2000]. It is measured in $W/(m^2 \times sr^1)$. On the way to the space, this radiant flux interacts with various atmospheric gases and particles. Thus *radiance-at-sensor* indicates the radiant energy recorded by the sensor which is affected by atmospheric scattering, absorption, reflection and refraction.

The task left to the user is to convert the radiance-at-sensor data first into true radiance and then to reflectance. True radiance is free from atmospheric distortions which affect radiant fluxes from the surface to the sensor. *Reflectance* is the dimensionless ratio between the radiant flux emitted by a surface and the radiant flux incident to it (the sun light) [Jensen, 2000]. We want to evaluate if reflectance is more effective in land use spectra characterization than radiance-at-sensor as it does not carry atmospheric distortions and accounts for the intensity of the incoming radiating energy.

Unfortunately, measurements of atmospheric parameters are rarely associated with remote sensed data. It is therefore necessary to retrieve their imprint on multispectral data through the data themselves and some other known parameters. Atmospheric correction models are able to retrieve indirectly these information and use them to estimate the surface reflectance.

The atmospheric correction model used in this study is FLAASH (Fast Line-of-sight Atmospheric Analysis of Spectral Hypercubes) by ITT-ENVI. FLAASH estimates directly also the reflectance value. Its prominent features are [ITT-ENVI Atmospheric correction module; Mattew *et al.*, 2003]:

- wavelength correction from the visible to the SWIR (short wave infrared) region (up to 3 μm);

- incorporation of MODTRAN4[19] radiation transfer code (this avoids using a pre-calculated database of modeling results);
- correction of spectral mixing;
- adjustable spectral polishing parameters;
- correction of images taken from both nadir or slant positions.

The ancillary information that need to be retrieved from the Header file are the exact day and time of flight, plane and mean ground elevation, coordinates of the scene centre, pixel size and some climatic and geographic descriptions (tropical, rural area, etc). For a step-by-step technical guide of the followed procedure see Appendix F. After performing atmospheric correction with FLAASH the noisy bands will be automatically excluded from the reflectance image.

5.3.3 Feature selection

Alternatively (or complementary) to atmospheric correction, it is possible to select the spectral bands that are most relevant for land use class determination. Normally, noisy bands will be discarded in this process, which is useful for reducing the size and processing time of large spectral data sets. Two are the selection approaches taken in this study: orthogonal transformation (PCA and MNF) and out-to-out band selection (with R and EnMAP Toolbox). Before proceeding in describing them, few definitions are clarified.

Spectral bands can be regarded as *features*, as features describe an object. Each pixel (the objects) can thus be represented as a point in a k-dimensional plot, called *feature space*, with k being the number of features [Tso and Mather, 2009]. *Orthogonal transformations* transform the feature space into a new set of axes with lower correlation. These axes are orthogonal to the originals and start at the data mean. The new number of axes can be

19 MODTRAN is a highly accurate program developed by Spectral Sciences, Inc. which models the electromagnetic propagation of atmospheric radiation [Berk *et al.*, 1998]. Currently, the latest available version is MODTRAN5.

lower or equal to the original data set; however, since the first axes display the highest decorrelation, it is often preferred to reduce the number of features. Orthogonally transformed images usually appear more colorful than color composites from spectral images because features are less correlated [Richards and Jia, 1999]. *Feature selection* on the other hand does not transform the feature space but simply ranks the bands according to their importance in determining the land use class.

Orthogonal transformations with PCA and MNF

The Principal Component Analysis (PCA) is a common technique to orthogonalize data sets. It ranks and transforms features according to the highest variance [Richards and Jia, 1999]. However, this does not imply that noisy bands are excluded. The Minimum Noise Fraction (MNF) transformation overcomes this problem by generating feature spaces that maximize the signal-to-noise ratio [Canty, 2010]. It is actually a double Principal Component transformation where first noise is isolated and rescaled and in the second step the remaining bands are regularly processed as in a PCA [ITT-ENVI, 2001].

Performing PCA and MNF transformations is a rather automatized process in ENVI and easy to perform. In both cases it is possible to select each time a different number of features (bands) to describe the final image. For more theoretical background on PCA and MNF see respectively Landgrebe [1998] and Green *et al.* [1988].

Feature selection in R

The package used in this study from the statistical program R is randomForest™ developed by Leo Breiman and Adele Cutler [Breiman, 2001]. A technical record of the steps follows in Appendix G. The two indexes used by randomForest to rank feature importance are the Mean Decrease Accuracy (MDA) and the Mean Decrease Gini (MDG). MDA ranks variables according to their difference in prediction accuracy. MDG is the normalized sum of all Gini decreasing impurities along a tree over the total number of trees [Calle and Urrea, 2011]. It is implicitly assumed that noisier bands will score low in the list.

Feature selection with EnMAP Toolbox

EnMAP Toolbox 1.1 is a software developed by Humbold University of Berlin and DLR (Deutsches Zentrum für Luft- und Raumfahrt) for multi- and hyperspectral data analysis. It is currently developed specifically for hyperspectral data from EnMAP, a German scientific satellite mission with envisaged launch in 2013. However with some modifications EnMAP Toolbox can process images from other remote sensing sources too.

Through EnMAP Toolbox it is possible to invoke imageSVM, an IDL tool for support vector machine regression and classification analysis based on LIBSVM by Chih-Chung Chang and Chih-Jen Lin [2011]. imageSVM is freely available for scientific purposes at: http://www2.hu-berlin.de/hurs/projects/imageSVM.php. Alternatively, imageSVM can run from the IDL Virtual Machine™ without necessarily owning a license for IDL or ENVI [Van der Linden et al., 2010a].

Feature selection is an indispensable part of data preparation in imageSVM. Since the band selection is mainly based on visual assessment, this method has some limitations for large hyperspectral datasets. However, it can be considered a potentially interesting complement to feature selection with ENVI and R. For familiarizing with imageSVM in this context see Appendix H.

5.4 Image analysis

5.4.1 Unsupervised classification

Unsupervised classification algorithms use statistical techniques to cluster k-dimensional data according to their spectral values [ITT-ENVI, 2001]. They require the user to input the number of desired clusters. Several such algorithms are available in ENVI and were applied in this study. For compactness and relevance reasons only the Gaussian Mixture algorithm is presented here.

Gaussian Mixture

The Gaussian Mixture is an iterative algorithm somehow superior to other unsupervised classification methods because it uses multivariate normal probability densities, thus allowing higher clustering flexibility [Canty, 2010]. This classification tool is only available in ENVI with the IDL extension. The algorithm used in this study is actually Canty's modified version of Expectation Maximization (EM) applied to a Gaussian Mixture model. Unfortunately this extension is not suited for large or high-dimensional data sets because it does not exploit the ENVI tiling facility; it allows though a more flexible algorithm parametrization.

5.4.2 Supervised classification

Contrary, supervised classification requires the user to select and input training areas, which are used to train the classifier. Though the procedure might be tedious, the results are ofter more satisfactory than those from unsupervised classification [Tso and Mather, 2009]. The disadvantage is that for defining the classes some prior knowledge on the study site is necessary.
Like for unsupervised classification, ENVI offers several options as algorithms. The two that gave the most promising results in this study are the Maximum Likelihood (ML) and the Support Vector Machine (SVM), which were implemented into 5 variants: standard ML and SVM in ENVI, ML and SVM with accuracy assessment modified by Canty [Canty, 2010] and SVM in EnMAP Toolbox.

Maximum Likelihood

The Maximum Likelihood classifier ranks the pixel belonging probability to each class and assigns the pixel to the class with the highest probability [Tso and Mather, 2009]. This assignation is based on the reflectance value or digital number per each band. ML classifier assumes that all classes have a normal probability distribution prior band analysis. However, developments of this algorithm not applied in this study proved that there is the potential to use expected class distribution or pixel context to improve the final ML classification accuracy [Strahler, 1980; Hubert-Moy *et al.*, 2001].

The decision rule used by ENVI ML classifier is [Canty, 2010; Richards and Jia, 1999]:

pixel g is in class i provided $d_i(g) \geq d_j(g)$ for all $j = 1 \ldots I$

given that the discriminant function is:

$$d_i(g) = -\log|\ \Sigma_i\ | - (g - \mu_i)^t\ \ \Sigma_i^{-1}\ \ (g - \mu_i)$$

The moments Σ_i and μ_i are directly estimated from the training data.

Due to the limited number of parameters estimations, the computational time is also limited [Canty, 2010]. Being a parametric model, ML strongly relies on the prior assumption of data structure. If the normal distribution assumption is correct, parametric models show stronger results as compared to non-parametric ones [Whitley and Ball, 2002].

ML classification in ENVI outputs also a gray-scale rule image consisting of the discriminant functions for each class and training observation [Canty, 2010]. In the case of ML the rule image values are the probability of pixel belonging to class. This rule image can be used to evaluate the classification and possibly to modify the discriminant thresholds [ITT-ENVI Tutorial: Classification methods; ITT-ENVI, 1999].

Support Vector Machine

Support Vector Machine (SVM) classifiers are state-of-the-art machine learning algorithms [Tso and Mather, 2010]. Like in ML methods, the structural misclassification error is minimized by accounting for data variance. But whereas in ML the variance is empirically estimated, SVM partitions the feature space by taking a subset of the training data (the support vectors) without invoking their distribution [Canty, 2010]. Being a non-parametric model, SVM has the advantage to fit well most data sets [Whitley and Ball, 2002]. Though SVMs were originally conceived for binary classification, a number of multiclass applications have been investigated [Hsu and Lin, 2002; Huang *et al.*, 2002; Foody and Mathur, 2004]. The multiclass approach used in ENVI to determine the membership class is regarded as a 'one-to-one' voting scheme [Canty, 2010].

SVM with EnMAP Toolbox

With EnMAP Toolbox-imageSVM described on page 29 is possible to classify an image using the SVM algorithm. Though the results should be very similar to SVMs applied in ENVI, in reality different adjustable model parameters can originate different outputs. In particular the user can modify the width of the Gaussian kernel function (parameter **g** in $K(x, x_i) = \exp(-g\ |x-x_i|^2)$ used to separate class distribution and control the training data individual influence (**C**) on classification [van der Linden *et al.*, 2010a].

ML and SVM by Canty

In addition to standard ML and SVM classification methods, also a modified version of both was applied. Canty [2010] in fact developed some ENVI/IDL extensions for standard classifications with a smart consideration for accuracy assessment.
Normally, the confusion matrix (chapter 5.4.3) is used to evaluate the classified map accuracy. ENVI built-in procedure:

- uses pixels from all training areas to calculate average band values per each class;
- these averages are used to classify the whole image (note: it can be that the final classification of some training pixels differs from the original assigned class);
- the confusion matrix is calculated by taking pixels from these training areas and compare them with the final classification.

Whereas Canty's variants:

- separate the pixels of all training areas into training and testing sets (in proportion 2:1);
- take the average band values of the training set to classify the whole image;
- the confusion matrix is calculated by comparing the testing pixels with the final classification.

Clearly the advantage of Canty's variant lays in the fact the testing pixels are completely independent from the training one, therefore the assessment is less bias.
Canty's ENVI/IDL extensions can be downloaded for free from his webpage (http://mcanty.homepage.t-online.de/software.html).

5.4.3 Accuracy assessment

Image analysis is not complete before an accuracy assessment is performed. Accuracy of thematic maps resulting from classification can be defined as the degree of correct representation of land cover. The most widely accepted assessment tool in image classification is the *confusion matrix* [Canty, 2010; Stehman, 1992; Tso and Mather, 2009]. The confusion matrix is an array of $i \times i$ dimension where i is the number of classes. The labels in the first row represent the training data classes whereas the labels in the first column represent the testing data classes. The cells in between represent the number of pixels assigned to each category. An example is illustrated in Fig. 8.

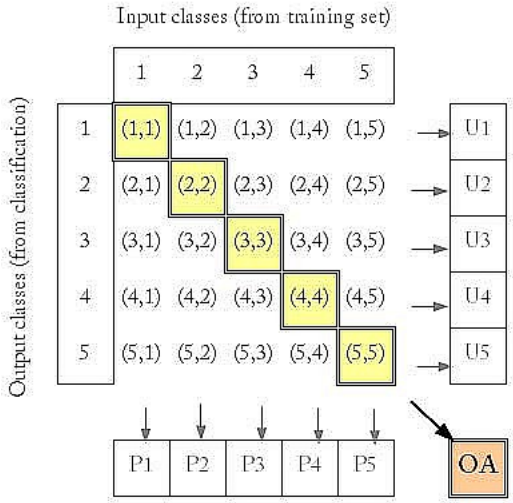

$OA = \Sigma \text{ diagonal} / \text{total}$

$P_i = (i, i) / \Sigma \text{ column } i$

$U_i = (i, i) / \Sigma \text{ row } i$

$$\kappa = \frac{(OA - \sum_{i=1}^{5} P_i \times U_i)}{\sum_{i=1}^{5} (P_i \times U_i)}$$

where i is a class number

Fig. 8: Confusion matrix of classification at 5 classes. Cells are indicated as: (row number, column number). P and U stand for Producer's and User's accuracy with the respective class number, OA for Overall Accuracy. K is the Kappa coefficient.

The *overall accuracy* is given by the diagonal sum (correctly classified pixels) divided by the sum of all pixels. Other accuracy indexes can be retrieved from the confusion matrix, such as the *producer's* and the *user's accuracy* per each class. These are respectively the ratio of pixels correctly assigned to one class over the total number of pixels that should be assigned to it (column sum) and the ratio of pixels correctly assigned to one class over

the total number of pixels that were assigned to it (row sum) [Tso and Mather, 2009].

Last but not least, from the confusion matrix it is possible to calculate the *Kappa coefficient*. Contrary to the producer's and user's accuracy, the Kappa coefficient **κ** takes into consideration all the information contained in the confusion matrix and corrects the classification rate for the probability of classifying pixels correctly by chance [Canty, 2010]. Alternatively to the equation given in Fig. 8 **κ** can be defined as:

$$\kappa = \frac{\Pr(\text{correct classification}) - \Pr(\text{chance classification})}{1 - \Pr(\text{chance classification})}$$

where *Pr* stands for probability [Tso and Mather, 2009]. **κ** is considered somehow more accurate than other indexes because provides two statistical tests of significance into one. It indicates in fact the degree of significant difference between the result of the classification and a random classification. Second, it can be used as reference for comparing two matrices, as in the case of classification algorithm evaluation. Although Stehman [1992] points that **κ** could slightly lose its assessing power when used in context other than simple random sampling, other authors [Congalton and Green, 1999; Foody, 2000; Li and Moon, 2004] used it for accuracy assessment also in systematic sampling. The confusion matrix accuracy assessment can be applied to both supervised and unsupervised classifications. Instead of the confusion matrix, it is possible to obtain an accuracy assessment also by reiteratively repeat the 'leave-one-out' test [Gretton et al., 2001; Kearns and Ron, 1999] (not applied in this study, though).

5.5 Post-classification processing

Some post-classification tools in ENVI can be used to improve the accuracy. These functions are named *Sieve*, *Clump* and *Combine Classes*. *Sieve* smooths the image by removing isolated pixels, after a minimum cluster size has been input. *Clump* merges similarity classified areas. *Combine classes* allows the user to join classes with very similar spectra into a more generalized one [ITT-ENVI Tutorial: Classification methods]. When appropriate, all three tools were tested over the classification results.

6 Results

6.1 Sampling design

A total of 207 sampling plots were digitized, belonging to 12 land use and cover classes. The number of selected reference pixels was 14 842 over a population of 490 000.

6.2 Data collection

198 polygons were actually field validated as the remaining 9 sites could not be accessed, leaving a total of 13 744 pixels to be used as reference areas. During field data collection the LUC labeling of 38 polygons and the shape of 17 ones was modified due to visual misinterpretation of the remote sensed images. The most commonly misattributed LUC classes from visual interpretation compared with field survey were: mixed tree-grassland (15), shade coffee at ≥3 strata (13), shade coffee at 2 strata (7). The LUC type changed in only in two sites between 2005 and 2011; it was anyway possible to trace back to the original land use, being mainly agricultural fields under crop or fallow rotation.

All GPS point and digital pictures acquired during data collection were incorporated into vector files using the QuantumGIS-eVis plugin (Appendix C).

6.3 Image processing

6.3.1 Georeferencing

The maximum observed spatial offsets between the georectified MASTER against the OpenStreetMap (OSM) layer and GeoEye1 mosaic were ±3 and ±4 pixels (30 and 40 m) respectively (Fig. 9). Surprisingly, the spatial offset between the GeoEye-1 manually georeferenced mosaic and the OSM layer was 10-15 m, lower than the dispatched original 5 band GeoEye-1 image (~20 m offset against OSM). On the other hand orthorectification of the GeoEye-1 standard product with the available DEM using ENVI 4.8 improved the spatial accuracy to ± 5-7 m.

Fig. 9: MASTER image (left) and GeoEye-1 mosaic (right) overlayed with OpenStreetMap (OSM) layer.

6.3.2 Atmospheric correction

From FLAASH one reflectance image was created and scaled for a factor of 10 000 (Appendix F). A sample spectra profile of the reflectance image compared to the original radiance-at-sensor is shown in Fig. 10. The 3 bands automatically excluded by FLAASH because classified as noisy were band 16, 17 and 18 (1.78 to 1.98 μm).

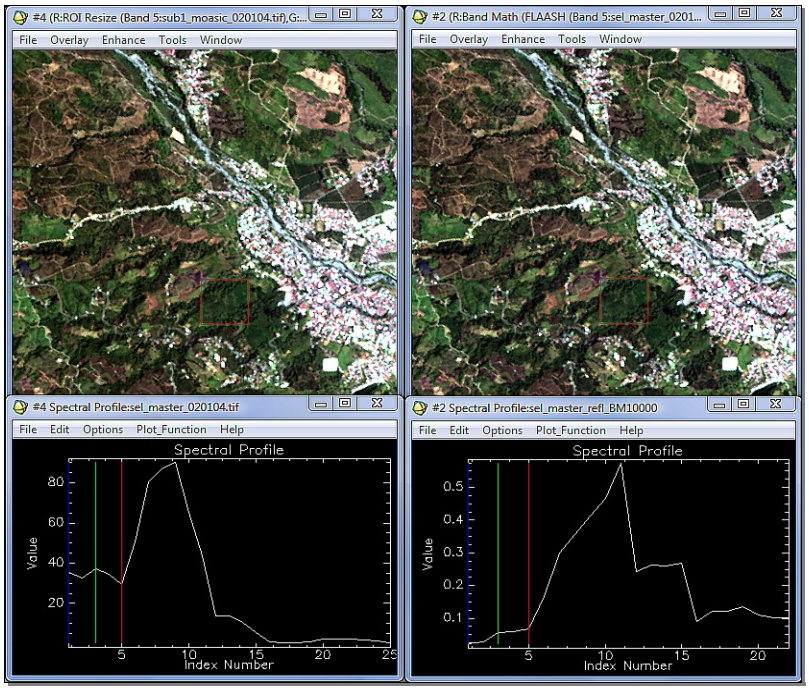

Fig. 10: Radiance (left) and FLAASH-reflectance (right) images of MASTER scene over Turrialba. The associated spectral profile refer to the same pixel. Index = band number.

6.3.3 Feature selection

From PCA and MNF analysis three images have been created: one PCA at 4 bands and two MNF at 6 and 25 bands respectively. The number of bands is subjectively chosen by the operator. However the aim was to condensate spectral information while preserving essential traits for classification.

The R-randomForest MDA and MDG ranking results are shown in Fig. 11.

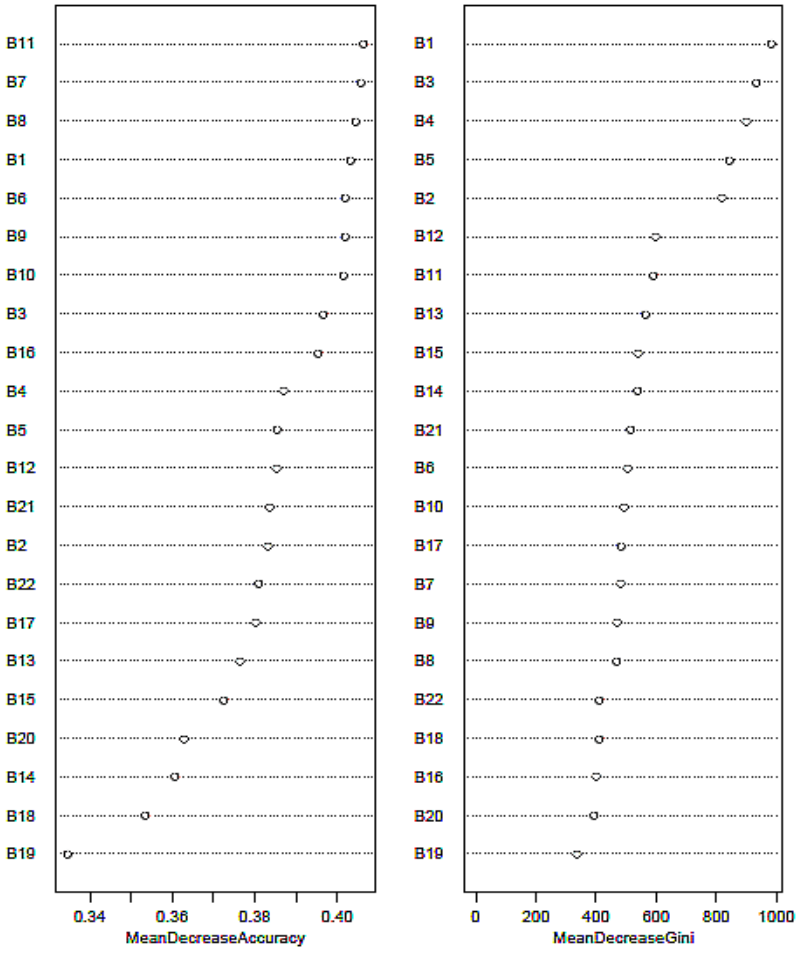

Fig. 11: Feature selection using the Mean Decrease Accuracy (MDA) and the Mean Decrease Gini (MDG) indexes available in R randomForest package. The bands (B) are ranked top-to-bottom according to the importance in determining the LUC class. Only 22 bands appear in each list, as the other 3 (23 to 25 in both cases) were considered less influential thus excluded. This forest was obtained using the first 25 bands of MASTER data, set seed= 4543, trees = 1000.

From these rankings the first 16 (MDA > 0.38) and 17 (MDG > 450) bands were selected. This means that the bands used for further processing from MDA index were all except 13 to 15, 18 to 20 and 23 to 25; and for the MDG index all except 16, 18 to 20 and 22 to 25.

Last, as mentioned in 5.3.3, EnMAP Toolbox does not provide a statistical comparison among bands. However EnMAP Toolbox (like ENVI on the other hand) offers the possibility of identify noisy bands by visual interpretation. A screen-shot with one significant band and the three noisy ones is presented in Fig. 12.

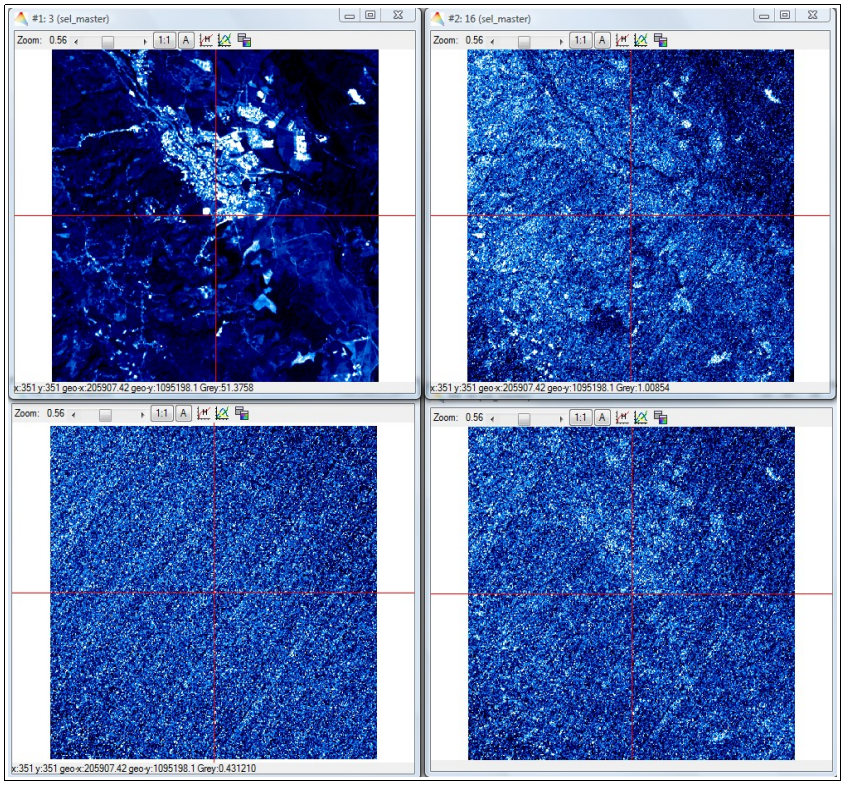

Fig. 12: Screen shot of 4 MASTER spectral bands displayed in EnMAP Toolbox. Clockwise from top left corner: band 3, 16, 17 and 18. The image is MASTER-1B (March, 11th 2005) over the study site in Turrialba, Costa Rica.

Only these 3 bands (16, 17 and 18) were classified as noisy in EnMAP Toolbox .

6.4 Image analysis

6.4.1 Results of unsupervised classification

The Gaussian Mixture algorithm could be applied only to images with reduced number of features. Therefore the algorithm was only tested on: PCA at 4 bands, MNF at 6 bands, first 5 bands of the radiance-at-sensor image and first 5 bands of the reflectance image[20]. The used parameters were: initial number of classes = 11; min threshold = 0 max threshold = 2. The output clusters were visually analyzed and confronted with the true color composite MASTER image and other thematic from supervised classification maps to facilitate interpretation; a land use label was assigned to the clusters, which in some cases were merged. The results were then tested in a confusion matrix against the reference ROIs created in 5.1.3. Note that only the identified LUC classes could be tested in the confusion matrix; this mean that each time a different number of test pixels was considered. The overall accuracies of these 4 Gaussian Mixture classifications and the relative Kappa coefficients are listed in Table 5.

Image	**No. bands**	**No. classes**	**No. tested pixels**	**OA**	**Kappa coeff.**
PCA	4	8	13339	46.4%	0.3732
MNF	6	8	12951	54.2%	0.4578
Radiance-at-sensor	5	7	12728	53.5%	0.4111
Reflectance	5	9	13562	42.8%	0.3210

Table 5: Overall accuracies (OA) and Kappa coefficients obtained from confusion matrices of 4 images classified with the Canty's modified version of Gaussian Mixture algorithm. *No. classes* indicates the total number of classes after merging and labeling tested in the confusion matrix. *No. tested pixels* indicates the total number of pixels from the reference ROIs which were used in the comparison. Initial parameters: number of classes = 11; min threshold = 0 max threshold = 2.

20 The algorithm can be applied only to floating-point images and not to the 2-byte integer scaled reflectance.

The required processing time for clustering was above 60 minutes[21]. No pixels were left unclassified, though unsupervised algorithms contemplate this possibility.

6.4.2 Supervised classification

As for the unsupervised case, also for supervised classification the algorithms were tested on all images. This was meant to evaluate both the need for atmospheric correction, feature selection and evaluate different classification algorithms. The confusion matrices of the highest scoring supervised classification algorithms are summarized in Table 6.

The three most accurate thematic maps are presented in Fig. 13. The graph showing the average spectral emission of different land use classes follows in Fig. 14 and Fig. 15.

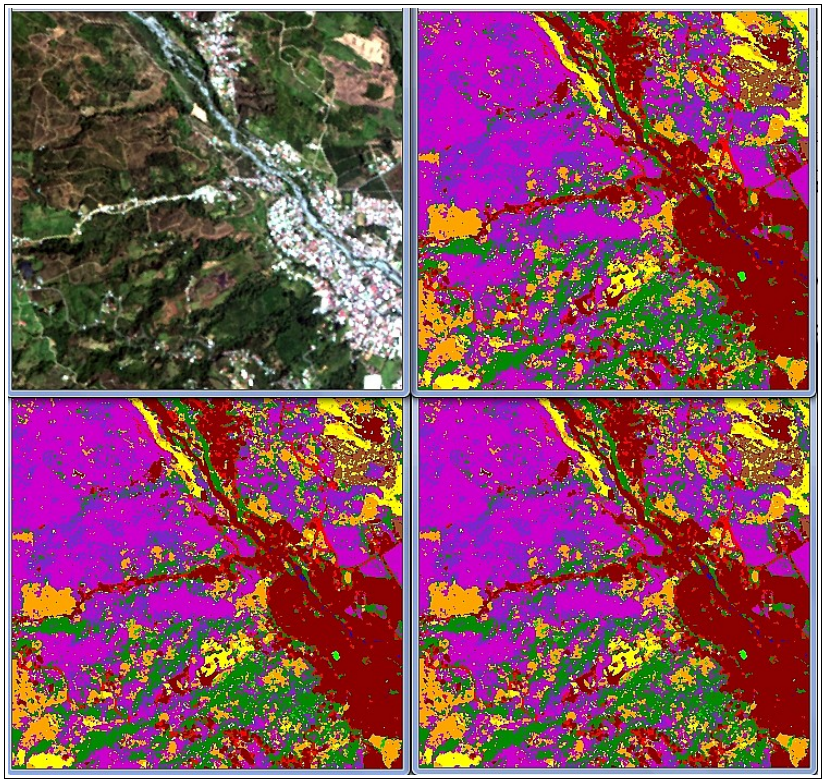

Fig. 13: Clockwise starting from the top left corner subset of: the original MASTER image over Turrialba; standard Maximum Likelihood (ML) in ENVI using the radiance-at-sensor MASTER image (25 spectral bands); Canty's modified ML classification of the same image; Canty's modified ML classification of MNF at 25 bands.

21 In a 32-bit processor, 2 GB RAM, 2.16 GHz.

Algorithm	Bands	Notes	Overall accuracy	Kappa coefficient
MaxLikelihood	22 (no 16 to 18)	Reflectance img	70.0%	0.6432
MaxLikelihood	22 (no 16 to 18)		71.7%	0.6638
MaxLikelihood	25		73.5%	0.6841
SVM	22 (no 16 to 18)	Reflectance img	68.0%	0.6085
SVM	22 (no 16 to 18)		68.3%	0.6109
SVM	25		68.5%	0.6144
Canty ML	22 (no 16 to 18)	Reflectance img	71.1%	0.6558
Canty ML	22 (no 16 to 18)		71.3%	0.6588
Canty ML	25		73.1%	0.6794
Canty SVM	22 (no 16 to 18)		67.5%	0.6016
Canty SVM	25		67.6%	0.6024
Canty ML	16 (MDA)		67.7%	0.6182
Canty ML	17 (MDG)		69.3%	0.6364
Canty SVM	16 (MDA)		66.6%	0.5906
Canty SVM	17 (MDG)		66.3%	0.5872
Canty ML	PCA (4)		48.8%	0.4199
Canty ML	MNF (6)		59.0%	0.5223
Canty ML	MNF (25)		73.1%	0.6789
En-MAP SVM	22 (no 16 to 18)	See (a)	71.1%	0.6790
En-MAP SVM	22 (no 16 to 18)	See (b)	64.6%	0.6069

Table 6: Summarizing table of overall accuracies and Kappa coefficients obtained from confusion matrices of several supervised algorithms. ML = Maximum Likelihood, SVM = Support Vector Machine, MDA = Mean Decrease Accuracy, MDG = Mean decrease Gini. **(a)** Min (g)=0.01; Max (g)=10; (g) and (C) Multipliers=2; Min (C)=1; Max(C)=10000. **(b)** Min (g)=0.01; Max (g)=1; (g) and (C) Multipliers=2; Min (C)=100; Max(C)=10000. The highlight rows indicates the highest accuracy scores. Results from different algorithm / band combination are not shown because of lower accuracies.

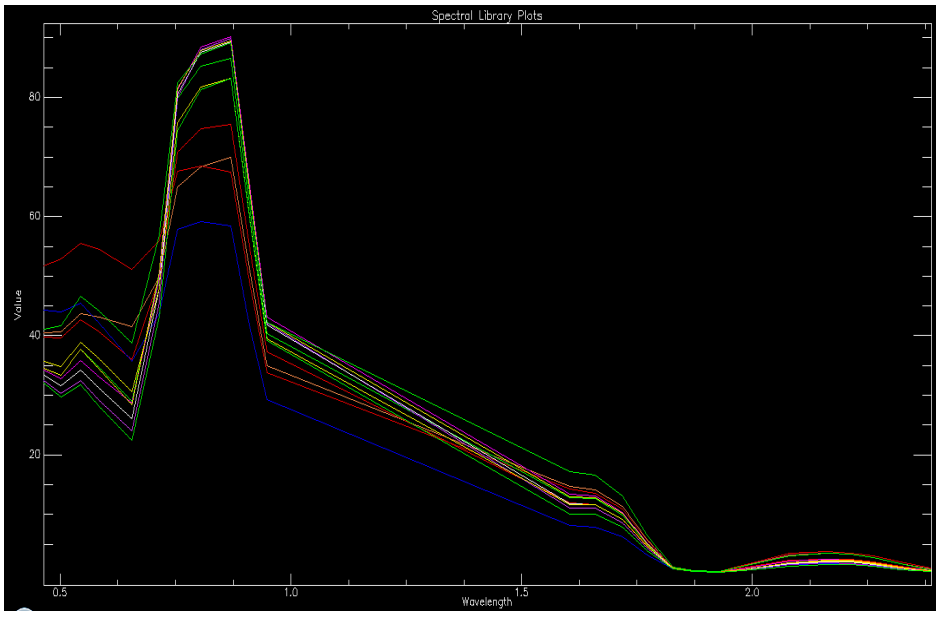

Fig. 14: Average land use class spectra of reference ROIs associated with MASTER radiance-at-sensor image (25 bands). Line colors correspond to the legend on page 17. Unit of the x-axis: wavelength (µm); y-axis: radiance (W m^{-2} sr^{-1}).

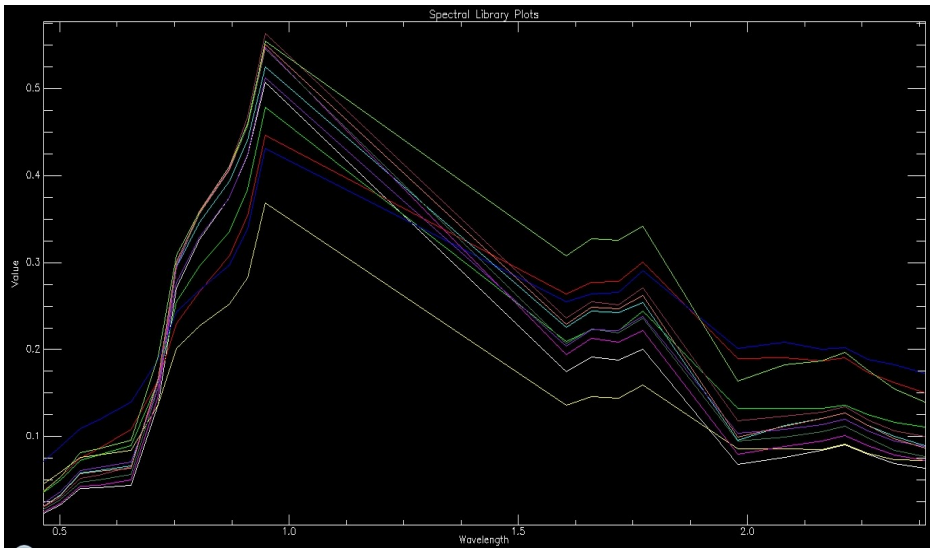

Fig. 15: Average land use class spectra of reference ROIs associated with MASTER FLAASH-reflectance image (22 bands). Line colors correspond to the legend defined on page 17. Unit of the x-axis: wavelength (µm); y-axis: reflectance ratio.

If we consider the computational effort PCA at 4 bands, MNF at 6 and 25 bands transformed images took in general slightly less time for classification processing as compared to the MASTER image at 22 and 25 bands in all classification algorithms. Time difference was more pronounced among algorithm types, with SVM classification being the slowest (approximately 30 minutes in ENVI vs about 1-2 minutes for ML)[22]. However SVM processing time in EnMAP Toolbox highly varied depending on the input parameters (especially sampling type, **g** and **C**). For the tested combinations it was in the range of 3 to 200 minutes[23].

6.5 Post-classification processing

The 3 most accurate classification images were first sieved and then clumped. The respective accuracy assessment results are presented in Table 7.

Algorithm	Image	Tool	Overall acc.	Kappa coef.
ML	MASTER 25 bands	sieve	72.7%	0.6765
		clump	74.8%	0.7002
Canty ML		sieve	72.3%	0.6712
		clump	73.8%	0.6889
	MNF 25 bands	sieve	72.2%	0.6706
		clump	73.8%	0.6887

Table 7: Overall accuracies and Kappa coefficients of 3 post-classified images. ML stands for Maximum Likelihood. MNF 25 for Minimum Noise Fraction at 25 bands. Clump was performed on the sieved image. Sieving parameters: 2 min. threshold, 8 number of neighbors. Clumping parameters: 3 operator size row, 3 cols. The highlight row shows the best combination in terms of accuracy.

22 In a 32-bit processor, 2 GB RAM, 2.16 GHz.

23 In a 64-bit processor, 16 GB RAM, 4 double processors.

Clumping was performed on the sieved image. In these case if clumping was performed prior sieving directly on the MASTER classified image the final accuracy would have been lower (results not shown). Sieving leaves some pixels unclassified; their number decreases after clumping but does not disappear.

At last we performed *Combine Classes* for the best sieved and clumped output (sieving and clumping of MASTER image classified with the standard ML algorithm). We started by analyzing carefully the confusion matrix (Fig. 16) and rule images (Fig. 17).

	Ground Truth (Percent)				
Class	tree crown co	barren land	paved road	building	water
Unclassified	1.60	1.20	0.90	1.09	0.00
tree crown co	65.14	0.00	0.45	0.00	0.00
barren land	0.33	88.43	0.00	0.07	0.00
paved road	0.87	0.00	88.34	1.89	0.00
building	2.65	0.00	4.04	85.96	0.00
water	0.00	0.00	0.00	1.24	98.68
sh coffee 3+	11.17	2.41	0.00	0.00	0.00
sh coffee 2	8.34	3.13	4.04	1.09	0.00
sun coffee	0.48	0.00	0.00	0.00	0.00
sugar cane	2.20	2.17	0.00	0.29	0.00
grassland	0.03	0.00	0.00	0.58	0.00
mixed tree-gr	7.19	2.65	2.24	7.78	1.32
Total	100.00	100.00	100.00	100.00	100.00

	Ground Truth (Percent)				
Class	sh coffee 3+	sh coffee 2	sun coffee	sugar cane	grassland
Unclassified	2.95	1.14	0.00	0.21	0.00
tree crown co	1.15	2.50	0.00	2.10	0.00
barren land	0.33	0.19	0.00	0.29	0.00
paved road	0.65	1.82	0.00	0.04	0.00
building	0.00	0.00	0.00	0.07	0.00
water	0.00	0.00	0.00	0.00	0.00
sh coffee 3+	83.96	7.19	0.00	1.96	0.00
sh coffee 2	6.55	77.67	0.78	3.71	0.00
sun coffee	0.00	1.63	99.22	0.25	0.00
sugar cane	2.78	1.63	0.00	81.53	0.00
grassland	0.00	0.00	0.00	0.00	100.00
mixed tree-gr	1.64	6.25	0.00	9.84	0.00
Total	100.00	100.00	100.00	100.00	100.00

	Ground Truth (Percent)	
Class	mixed tree-gr	Total
Unclassified	2.68	1.35
tree crown co	7.84	17.91
barren land	0.10	2.88
paved road	2.34	2.58
building	5.83	10.21
water	0.00	0.67
sh coffee 3+	1.72	8.55
sh coffee 2	11.51	20.02
sun coffee	0.10	1.42
sugar cane	7.69	18.88
grassland	0.00	0.45
mixed tree-gr	60.20	15.09
Total	100.00	100.00

Fig. 16: Confusion matrix of sieved & clumped MASTER radiance-at-sensor image (25 spectral bands) classified with ENVI ML algorithm using 11 LUC classes. The shown part of the confusion matrix indicates the matches between the testing (column) and the training (row) areas expressed in percentage. Overall accuracy: 74.8%; Kappa Coefficient: 0.7002.

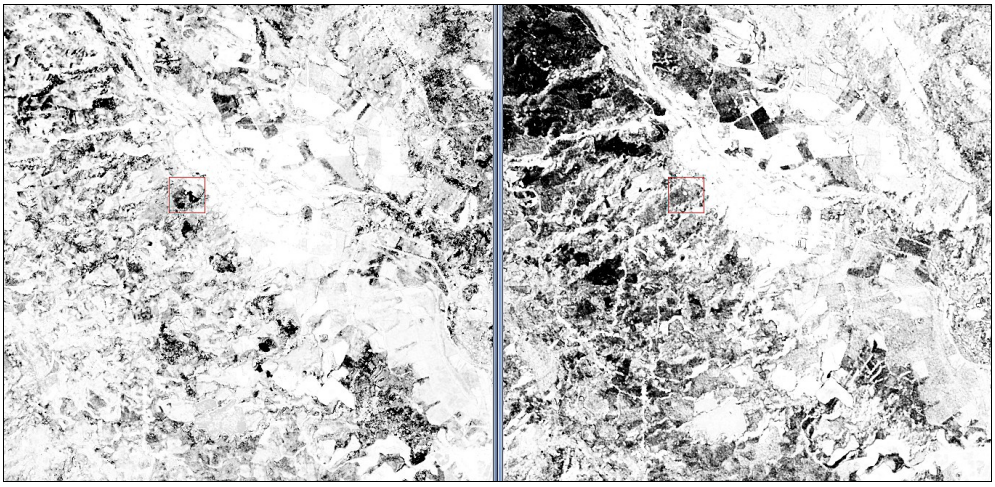

Fig. 17: Examples of rule images resulting from ML classification of MASTER reflectance scene. On the left: rule image of class 2 (shade coffee at ≥3 strata). On the right: rule image of class 3 (shade coffee at 2 strata). Dark pixels indicate higher probability of class belonging.

The class matches with less than 74.8% overall accuracy value are: tree crown cover and mixed tree-grassland. Tree crown cover is often confused with: shade coffee at ≥3 strata (11%), shade coffee at 2 strata (8%) and mixed tree-grassland (7%). Because the aim is to distinguish these categories, the class tree crown cover was left untouched.

Mixed tree-grassland is misclassified with: shade coffee at 2 strata (12%), tree crown cover (8%), sugar cane (8%) and building (6%). Since these classes have little management use in common they were preserved too.

To reduce the number of classes the two shade coffee classes were merged together into one class called *shade coffee*; and the class paved road was merged with building into a new category called *settlement*.

The comparison between the combined class image and the merged ROIs[24] gives overall accuracy of 76.7% and Kappa coefficient of 0.7127. For specific class accuracy in percentage refer to Fig. 18. The class shade coffee was classified respectively with 86%

24 See Discussion 7.4 for details.

and 71% producer's and user's accuracy. As mentioned before, some pixels (1.4%) were left unclassified after the sieving step.

	Ground Truth (Percent)				
Class	tree crown co	barren land	settlement	water	sh coffee
Unclassified	1.60	1.20	1.07	0.00	1.48
tree crown co	65.14	0.00	0.06	0.00	2.25
barren land	0.33	88.43	0.06	0.00	0.22
settlement	3.52	0.00	88.43	0.00	1.60
water	0.00	0.00	1.07	98.68	0.00
sh coffee	19.51	5.54	1.51	0.00	85.88
sun coffee	0.48	0.00	0.00	0.00	1.33
sugar cane	2.20	2.17	0.25	0.00	1.85
grassland	0.03	0.00	0.50	0.00	0.00
mixed tree-gr	7.19	2.65	7.04	1.32	5.40
Total	100.00	100.00	100.00	100.00	100.00

	Ground Truth (Percent)				
Class	sun coffee	sugar cane	grassland	mixed tree-gr	Total
Unclassified	0.00	0.21	0.00	2.68	1.35
tree crown co	0.00	2.10	0.00	7.84	17.93
barren land	0.00	0.29	0.00	0.10	2.89
settlement	0.00	0.11	0.00	8.17	12.74
water	0.00	0.00	0.00	0.00	0.67
sh coffee	0.78	5.67	0.00	13.23	28.54
sun coffee	99.22	0.25	0.00	0.10	1.42
sugar cane	0.00	81.53	0.00	7.69	18.90
grassland	0.00	0.00	100.00	0.00	0.45
mixed tree-gr	0.00	9.84	0.00	60.20	15.11
Total	100.00	100.00	100.00	100.00	100.00

Fig. 18: Confusion matrix of sieved and clumped MASTER image classified with ML modified algorithm after 2 LUC classes have been merged. The shown part of the confusion matrix indicates the matches between the testing (column) and the training (row) areas expressed in percentage.

7 Discussion

7.1 Sampling design

Implementing a systematic sampling scheme has several advantages: it requires no prior knowledge on the area; it is simple to explain to the field crew and to the reader; the observation units are spread homogeneously over the area and thus less autocorrelated; all parts of the population are covered, assuming that there is no cyclic land use distribution [Kleinn, 2007]. There is however the risk of under or over-represent some classes: for example too few reference pixels belonging to rare classes are collected to train properly the classifier or too many energies are invested in digitizing the umpteenth polygon which does not contribute in increasing information on that land type [Plourde and Congalton, 2003].

Thus considering the purpose of LUC classification and the drawbacks of systematic sampling, it could be possible to apply a *stratified sampling* scheme in further studies, as it would guarantee that all land use classes are represented equally. In stratified sampling homogeneous objects on the ground are isolated and visually classified. Object isolation can be performed through segmentation, followed by semi-automatic classification (best suitable for high spatial resolution images); alternatively, unsupervised classification can also work to identify land cover with similar spectra in lower resolution products. The selection of the objects to be sampled can be random or follow a(n) (un-)aligned scheme [Fitzpatrick-Lins, 1981].

One disadvantage of stratified sampling is that transport logistic, plot location and permission to access the sites might balanced out the time savings from manual polygon digitization of the whole quadrants. In addition in the case of unsupervised clusters labeling it is possible to perpetrate systematic observer bias if the operator is not familiar with the study scene, thus leading again to an unbalanced number of samples per class. However a successful implementation of stratified random sampling scheme was done for example by Foody *et al.* [2006], who also suggest 4 interesting tricks to reduce sample

size when the focus is on one class only.

The population size of this study was not random, as 49 km^2 is the minimum required area for ordered GeoEye-1 or IKONOS satellite imagery. This is an important factor to consider if the research is extended using different sensors or sites.

The sampling grid orientation was North-South and this could be arguably objected as user bias choice. However, if there is not a cyclic pattern in the landscape (e.g. systematic arrangements of sugar cane fields at 1200 m distance in the North-South direction), the error variance of the land use classes should not be much higher than from a sampling grid randomly oriented [Kleinn, 2007]. Moreover, it is easier to visualize and explain a systematic grid with cells oriented North-South rather than one oriented at different azimuths. Therefore, from the trade-off between increased error variance and higher practicality, we decided to apply a North-South orientation.

From a practical point of view the *grid cell size* (200 × 200 m) appeared to be suitable for the objective of land use observation around Turrialba, as each quadrant could be easily surveyed. However, the spectral variance among polygons of the same LUC class but belonging to different quadrants could be statistically studied using the intracluster correlation coefficient. This information should help in finding unconsidered spatial autocorrelation and be potentially incorporated into a stratified sampling scheme.

A way to increase statistic accuracy might be to switch the *square systematic grid* to a triangular one (this leads to a systematic unalignment of plots). Though the precision increases as the observation points are scattered even more homogeneously over the area, the square grid is just slightly less precise [Kleinn, 2007]. Therefore for simplicity a square grid is often preferred.

As referred in the methodology, several are the formulas proposed in the literature to estimate the *sample size* for remote sensed data within a certain confidence level. For Mather [2004] rule of thumb 30 × 25 bands = 750 pixels should be sampled per class; this gives a total of 8250 pixels (750 × 11 classes), below our sample size of 13 744. Before data collection other formulas were not possible to apply as no variance

estimations were available. After classification it is possible to obtain statistical information on the processed data, in particular the class standard deviation, covariance and correlation per each band (using ENVI Class Statistics). However, due to handling complexity of considering 25 spectral bands, spectral autocorrelation of neighboring pixels, feature space correlation, class distribution, definition and separability and lack of literature on the topic it was not possible to evaluate the chosen sample size or infer on the appropriate one within this study. It would be extremely fascinating to read in the future of studies on the topic.

Once the sampling scheme and sample size have been selected, for classification purposes it is also important to consider the sample placement and cluster size. Plourde and Congalton [2003] suggest to create training samples in homogeneous areas rather than selecting larger clusters which include many mixed pixels. Testing this effect on accuracy would be interesting by comparing our classification results with those from new digitized sampling polygons where all the edge pixels have been discarded. When evaluating these results it is however important to consider possible sample size differences, as the quadrants might no longer be wholly classified.

Congalton [1988] moreover showed that the size of each training areas should not be larger than 10 pixels, as no information is added by extra contiguous pixels. This is due to spectral correlation and reinforces the suggestion to digitize smaller plots within the original ones.

7.2 Data collection

The major issues faced in the field by applying the response protocol were in order: (i) *plot access* and (ii) *location of the sampling plot* in the ground. For the former it is very important to consider legal and security issues, as access to private land is not always possible. Distinctive signs such as an official car or a disclaimer document should help in most cases.

To locate more easily the plot an idea is to follow the path to reach it on a topographic map or a digital support such as Google Earth™. It was in fact experienced during the

field work that access to the Google Earth platform is possible even without internet connection, given that the program was preliminary opened roughly on the area of interest. In this way also the zooming in/out tool remains active.

Recording the camera height as described in the field manual (Appendix I) can be time demanding when the plots are numerous and superfluous for the objectives, so it can be omitted in similar studies.

No *error assessment* [Van Genderen *et al.,* 1978] was conceived for evaluating the accuracy of field data, the main reason being the simplicity of the legend applied. However it is recommended to employ at least two operators for the field data collection in order to reduce even more chances of error in plot location and/or class attribution.

Time gap between the sensed image and the field data collection is an issue to be taken into account. In our case, though the gap was 6 years, the land use management had not changed much. Only one site (consisting of 2 digitized plots) was converted from presumed pasture to tree plantation and was thus not possible to validate. In all other instances it was mainly a seasonal change rather than a change in land use (e.g. sugar cane fields were harvested when in the MASTER image they resulted still green or viceversa). In such cases it is important to adhere to the image interpretation as it is the image which will be processed.

When there is the need of assessing the *usefulness of data collection*, digitizing land use polygons before going to the field could provide a valuable basis for comparison with the field data. Considering the proportion of changed land use class (about 1 out of 5) and polygon shape (1 out of 12), it appears clear the need for field sampling in this study.

7.3 Image processing

It is very hard if not virtually impossible to achieve 100% geospatial accuracy in a map. Even the used OpenStreetMap (OSM) layers which were taken as spatial reference might contain geometric inaccuracies. These can be due to the GPS receiver positional error and/or low density of recorded points. However we assume these errors to be

limited as compared to automatized georectification of large images (such as the MASTER tile) or manually georeferenced images (as in the case of the GeoEye-1 mosaic). In addition it has to be mentioned that the latter carries small overlapping errors occurred during mosaicing. Thus the best available spatial reference were the OSM layers.

30 and 40 m spatial offset between the MASTER and respectively the OSM layer and GeoEye-1 mosaic indicate that there is room for geospatial improvements. On the other hand for the purposes of this study it is possible to accept this misregistration as the only images that were actually compared were the georeferenced MASTER image and the deriving thematic maps (which obviously match exactly). In future studies, if land use changes have to be detected over time, it is important to keep in mind the positional accuracy and matching of the analyzed maps. For ideas how to improve it see chapter 9 Outlooks.

When considering larger study areas, cloud cover and haze might require tile mosaicing. It is possible to conduct this operation with ENVI, however care should be taken when analyzing and processing the resulting mosaic. In fact different illumination conditions can affect further processing outputs. Therefore, in mountainous terrain with steep slopes topographic normalization should be applied. Also, to create a more homogeneous image it is recommended to atmospherically correct the mosaic (for example with the ENVI extension IR-MAD[25] [Canty and Nielsen, 2008] or with FLAASH model in ENVI), with one manual method (like Empirical Line Calibration or Flat Field) and/or by matching the image histograms using for example ERDAS-Imagine. The 'feathering' option in ENVI [ENVI Tutorial: Mosaicking] seems in fact too simplistic and does not solve the problem throughout but just in the overlapping area.

The described atmospheric correction models assume the Earth surface being flat and having a Lambertian reflectance behavior [Tso and Mather, 2009]. In this way the radiance pixel values are homogeneously corrected throughout the image, without taking

25 Interatively Re-weighted Multivariate Alteration Detection.

into account that different elevations and roughness of the landscape cause different solar incident and radiance angles. Though not applied in this study, two top methods for topographic correction are suggested: band ratioing and the Minnaert method [Colby, 1991; Law and Nichol, 2004; Tso and Mather, 2009]. Both take into account the satellite position as well.

Despite the promising results by Matthew *et al.* [2003], the reflectance image atmospherically corrected using FLAASH did not perform better than the radiance-at-sensor image (Table 6) and was therefore abandoned during classification. The need for atmospheric correction of a satellite scene of one acquisition date can be called in question if no accuracy benefits arise from it. However, a deeper analysis of the methodology applied could reveal involuntary misuse of the model. For suggestions how to improve the application of FLAASH see Outlooks.

In addition, other atmospheric modeling techniques could be tested, like Atmospheric CORrection Now (ACORN) and ATmospheric REMoval (ATREM). ACORN uses MODTRAN4 radiative transfer code like FLAASH for estimating atmospheric parameters, but contrary to the latter it retrieves water vapor concentration using bands 0.94 and/or 1.15 μm [Kruse, 2004]. ATREM[26] on the other hand is based on a 6-S atmospheric correction code, improved by Vermote *et al.* [1997] and briefly discussed in Tso and Mather [2009]. A comparison of these 3 atmospheric modeling techniques is given by Kruse [2004].

There are some proves that empirical methods such as DOS (Dark Object Subtraction) and ELC (Empirical Line Calibration) could perform better than theoretically superior but generalized models in calibrating remote sensed images [for DOS see Lu *et* al., 2002; for ELC see Karpouzli and Malthus, 2002], though the issue is still debated [Smith and Milton, 1999; Mahiny and Turner, 2007]. Empirical techniques require some knowledge of ground conditions, which have to be retrieved either from the image itself (in DOS) or by ground measurements (also subsequent, in ELC) [Tso and Mather, 2009].

As last remark for atmospheric correction we can conclude that FLAASH model was

26 ATREM is not available in ENVI, but see ITT-ENVI [2001].

superfluous in this study, the main two reasons being the poorer performance in classification and the fact that actually no comparison among different time scenes was required.

In feature selection both FLAASH-ENVI and EnMAP Toolox pointed as bands 16, 17 and 18 as noisy (1.803 to 1.953 μm). This is conform to the knowledge that water is absorbed by the atmosphere of electromagnetic wavelength of channels that span around 1.45, 1.95 and 2.50 μm [Jensen, 2000].

The R-package randomForest proved to be somehow less effective in identifying noisy bands in this study. The Mean Decrease Accuracy and Mean Gini Accuracy indexes showed no accordance (Fig. 11) and no apparent accuracy benefit arose from choosing the best appointed bands for classification (Table 6).

7.4 Image analysis

As mentioned in chapter 4, the legend applied it is clearly suited for the considered study site and should require modifications if extended to a different area. The classification scheme suggested on page 16 should provide the backbone for modifications. It has been shown that by reducing the number of classes the classification accuracy increases: therefore we suggest to keep the legend as condensed as the objectives allow or, alternatively, to merge some classes at the end of the classification.

The most prominent classification misattributions arising from the confusion matrices belong to the classes tree crown cover and mixed tree-grassland. This might be imputed to the legend and scale of observation: polygons were in fact defined as pixel spatial clusters irrespectively of their size provided that the LUC was homogeneous. This means that if there were trees in a grassland field (e.g. pasture), the area was classified in one polygon as mixed tree-grassland. In the case of MASTER medium spatial resolution images with many mixed pixels this can be accepted, as long as within the digitized polygon no pixel cluster larger than a certain size (e.g. 3×3) could fall into a different class. If this is the case, it would be appropriate to re-shape the polygon or revise the

legend. Thus in future studies we recommend: first of all to digitize only pure pixels or pixels whose LUC is unambiguous. Second, to clearly define the size of the legend unit, as this is crucial both for the classification accuracy and for the class definition. Alternatively, if the spatial resolution allows, 'in-between' classes (such as mixed tree-grassland or shade coffee) can be omitted and eventually only at the end created by merging neighboring pixel clusters (e.g. tree crown cover pixels merged with grassland or coffee clusters within a specified spatial distance into a new class).

Generally, all supervised classifications led to higher accuracies than the unsupervised Gaussian Mixture. This result agrees with similar findings in literature [Richards and Jia, 1999; Tso and Mather, 2009]. Conceptually, unsupervised classification is a rigorous method because classifies pixels purely according to their spectra and is not subject to the user's interaction. However since in our case different classes have little spectra variations (Fig. 14), training the classifier with reference areas in supervised classification outputs the best results. In terms of processing time ML was above all the fastest, making the Gaussian Mixture and SVM more demanding to implement.

Among supervised algorithms the one that performed best was Maximum Likelihood (Table 6). It has to be considered on the other hand that the accuracy indexes in a confusion matrix only refer to that specific thematic map and cannot be generalized. Most scientific efforts focus nowadays on machine learning algorithms, like SVM or artificial neural network, for their promising potentials [Erbek *et al.*, 2004; Huang *et al.*, 2002]. In addition some authors [Malinverni *et* al., 2011; Walter, 2004; Yu *et al.*, 2006] embraced object-based classifications (rather than based on single pixels) with positive results.

Canty's modified accuracy assessment lead to slightly lower results than the ENVI standard accuracy tests. The modified Canty's algorithms were repeated a number of times and the accuracy indexes kept on being lower than when all reference pixels were used as training set. Probably the 1/3 reference data excluded in Canty's variant from the training set did contribute to better train the classifiers. One possible explaination could be the high spectral variance *within* each LUC class. This needs further investigations,

targeting both the minimum sample size, the reference area selection and the legend. Very interesting would also be to analyze the spectral variability and overlapping *between* LUC classes in order to evaluate their separability. In the case of vegetation classification special relevance might take in this context a NDVI[27] band composite. One possible way to investigate and minimize class variance could be through the 'bootstrap' method [Efron and Tibshirani, 1986; McRoberts and Meneguzzo, 2007].

PCA and MNF did not perform better than the raw image in none of the classifications in terms of accuracy. However, the orthogonal transformations at 4 and 6 bands did require less processing time as expected. Considering the aim of the study, the size of the study area and the limited number of visible-near and short wave infrared (VNIR-SWIR) bands, we would not recommend to manipulate the feature space.

There is not yet clear consensus in the literature on the thresholds above which to consider a classification map accurate. Thomlinson *et al.* [1999] proposes 85% as Overall Accuracy and no class less than 70%. The considered MASTER image with 10 m spatial resolution showed to have high potential in this regard for shade coffee agroforestry systems detection in the region (classified respectively with 86% and 71% producer's and user's accuracy). The possible reasons why 86% of the shade coffee pixels were correctly detected whereas only 71% of the pixels classified as shade coffee were actually belonging to that class, is probably linked with the mistake mentioned at the beginning of this sub-chapter (alias the existence of class mixed tree-grassland).

Interestingly was the fact that not always sieving and clumping different classification results improved the accuracy. Sometimes both were useful, others clumping would increase the accuracy only if applied on the sieved image (pg. 43), others it would do it only when applied directly on the original classification and other times both decreased the accuracy. No particular pattern could be identified which linked the first classified

27 Normalized Difference Vegetation Index. It is given by the reflectance value ratio: $\frac{NIR - VIS}{NIR + VIS}$ were *NIR* is the near infrared and *VIS* is the red visible region of electromagnetic spectrum. In MASTER they would be channel 7 to 11 and 5 respectively [see also Li and Moon, 2004].

image and the post-processing results. We recommend therefore to test each time the accuracy through the confusion matrix when undertaking sieving and clumping.

Combine classes on the other hand proved to have more tangibly effects in all circumstances (+1.9% and +0.0125 overall accuracy and Kappa coefficient respectively). This follows the knowledge that decreasing the number of classes increases the overall accuracy. When ENVI merges two classes it operates on the classified image, not on the ROIs. To calculate the confusion matrix of the image with combined classes is therefore necessary to merge the ROIs. Note that a new ML classification based on the merged ROIs would output a different classification map from the combined class image, not only in accuracy terms but also in pixel class attribution. No unclassified pixels would result taking this approach since no sieving is contemplated.

8 Conclusion

The aim of this work was to test the potentials of LUC classification using MASTER airborne imagery. Special attention was paid to the class coffee-banana agroforestry systems. The results are very promising with 77% overall accuracy and 86% (producer's) and 71% (user's) accuracy for the shade coffee agroforestry class.

As sampling frame for reference data collection a systematic square grid was applied; all land within the selected sampling quadrants was manually digitized by visual interpretation using the MASTER and high spatial resolution GeoEye-1 image published in GoogleEarth. The classification key discussed and described in the legend could be applied to all sampled plots. However it was realized that defining the size of the areas to label is crucial. The sample size for this pilot study is discussed and referred to further analysis. The data collection methodology proposed is rather economical in terms of resources and easy to implement by one/two operators. Stratified sampling is suggested as alternative approach.

Among the tested classification algorithms supervised methods performed better than unsupervised ones in terms of accuracy and in some cases also processing time. Among the former the standard ENVI ML lead to the highest accuracy, followed (in order) by Canty's modified accuracy assessment for ML, SVM in EnMAP Toolbox, standard SVM and Canty's modified accuracy assessment for SVM.

In order to reduce data size the most relevant bands for spectral land use determination were researched. In particular, two orthogonal transformations (PCA and MNF), two out-to-out feature selections (with R and EnMAP Toolbox) and FLAASH atmospheric correction model were applied. Surprisingly, none of these attempts performed better than the full MASTER image at 25 bands, calling for further investigations.

Accuracy was mainly improved by post-processing operations, particularly sieving & clumping (+1.3%) and class combining (+1.9%). Ideas for possible study developments are referred to the Outlooks chapter.

9 Outlooks

- Analysis of MASTER TIR bands for land use classification [French et al., 2000; Keuchel et al., 2003; Nemani and Running, 1997];
- comparison of classification algorithms and outputs with images taken from other sensors [see for example Xie *et al.*, 2008];
- comparison of MASTER classification performance using other CARTA mission sensors;
- georectification of MASTER image using the available DEM and topographic correction;
- for atmospheric correction with FLAASH: change of atmospheric parameters, possibly retrieved from other sources;
- other atmospheric correction options: ATREM, ACOR, Dark Object Subtraction, use of EFFORT, Empirical Line Calibration, Flat Field correction, IARR (Internal Average Relative reflectance calibration), Multivariate Alteration Detection (MAD), QUAAC, Temporally Invariant Cluster (TIC, Chen *et al.* [2005]), modules is ERDAS-IMAGINE, buy a Lever-3A product;
- investigate on sample size of multispectral geospatial data;
- improve polygon digitization by excluding ambiguous pixels. No pixel spatial sub-cluster within each polygon should be able to fall into another LUC class;
- object-based classification: segmentation, object extraction module in ENVI-EX (called feature extraction module);
- apply a stratified sampling scheme;
- feature selection: n-D Visualizer, create new bands e.g. NDVI or other ratios [Plourde and Congalton, 2003], perform band correlation analysis;
- extract endmembers: Pixel Purity Index (PPI), SMAAC;

- investigate potential spatial correlation between classes, e.g. through the bootstrap method [McRoberts and Meneguzzo, 2007];
- for classification: try Spectral Angle Mapper (SAM), Artificial Neural Networks, fuzzy methods, Decision Trees, un-/supervised mixed classifications, Gomez *et al.*, [2010];
- combine soil data for land use potentials and correlation finding. In addition, soil, agroforestry and FOC mapping should go arm-in-arm as the fungi propagates through the soil;
- extend the study to areas with pure coffee and pure banana plantations and larger agroforestry range for comparison;
- test of Canty's `CT_RUN` accuracy assessment against ENVI confusion matrix.

10 Appendices

10.1 Appendix A

FAO Forest Resource Assessment (FRA) legend [FRA, 2010]

TERM, definition and explanatory notes
FOREST **Land spanning more than 0.5 hectares with trees higher than 5 meters and a canopy cover of more than 10 percent, or trees able to reach these thresholds *in situ*. It does not include land that is predominantly under agricultural or urban land use.** Explanatory notes 1. Forest is determined both by the presence of trees and the absence of other predominant land uses. The trees should be able to reach a minimum height of 5 meters *in situ*. 2. Includes areas with young trees that have not yet reached but which are expected to reach a canopy cover of 10 percent and tree height of 5 meters. It also includes areas that are temporarily unstocked due to clear-cutting as part of a forest management practice or natural disasters, and which are expected to be regenerated within 5 years. Local conditions may, in exceptional cases, justify that a longer time frame is used. 3. Includes forest roads, firebreaks and other small open areas; forest in national parks, nature reserves and other protected areas such as those of specific environmental, scientific, historical, cultural or spiritual interest. 4. Includes windbreaks, shelterbelts and corridors of trees with an area of more than 0.5 hectares and width of more than 20 meters. 5. Includes abandoned shifting cultivation land with a regeneration of trees that have, or is expected to reach, a canopy cover of 10 percent and tree height of 5 meters. 6. Includes areas with mangroves in tidal zones, regardless whether this area is classified as land area or not. 7. Includes rubber-wood, cork oak and Christmas tree plantations. 8. Includes areas with bamboo and palms provided that land use, height and canopy cover criteria are met. 9. Excludes tree stands in agricultural production systems, such as fruit tree plantations, oil palm plantations and agroforestry systems when crops are grown under tree cover. Note: Some agroforestry systems such as the "Taungya" system where crops are grown only during the first years of the forest rotation should be classified as forest.
OTHER WOODED LAND **Land not classified as Forest, spanning more than 0.5 hectares; with trees higher than 5 meters and a canopy cover of 5-10 percent, or trees able to reach these thresholds *in situ*; or with a combined cover of shrubs, bushes and trees above 10 percent. It does not include land that is predominantly under agricultural or urban land use.** Explanatory notes 1. The definition above has two options: • The canopy cover of trees is between 5 and 10 percent; trees should be higher than 5 meters or able to reach 5 meters *in situ*. or • The canopy cover of trees is less than 5 percent but the combined cover of shrubs, bushes and trees is more than 10 percent. Includes areas of shrubs and bushes where no trees are present. 2. Includes areas with trees that will not reach a height of 5 meters *in situ* and with a canopy cover of 10 percent or more, e.g. some alpine tree vegetation types, arid zone mangroves, etc. 3. Includes areas with bamboo and palms provided that land use, height and canopy cover criteria are met.

TERM, definition and explanatory notes
OTHER LAND **All land that is not classified as Forest or Other wooded land.** Explanatory notes 1. Includes agricultural land, meadows and pastures, built-up areas, barren land, land under permanent ice, etc. 2. Includes all areas classified under the sub-category "Other land with tree cover".
OTHER LAND WITH TREE COVER (*sub-category of OTHER LAND)* **Land classified as Other land, spanning more than 0.5 hectares with a canopy cover of more than 10 percent of trees able to reach a height of 5 meters at maturity.** Explanatory notes 1. The difference between Forest and Other land with tree cover is the land use criteria. 2. Includes groups of trees and scattered trees in agricultural landscapes, parks, gardens and around buildings, provided that area, height and canopy cover criteria are met. 3. Includes tree stands in agricultural production systems, for example in fruit tree plantations and agroforestry systems when crops are grown under tree cover. Also includes tree plantations established mainly for other purposes than wood, such as oil palm plantations. 4. Excludes scattered trees with a canopy cover less than 10 percent, small groups of trees covering less than 0.5 hectares and tree lines less than 20 meters wide.
INLAND WATER BODIES **Inland water bodies generally include major rivers, lakes and water reservoirs.**

10.2 Appendix B

Simplified version of Raunkiær's life form classification

The following appendix is meant to be consulted in case of doubt when classifying life forms or for the interested reader. In the present work we distinguished vegetation types in the following three main categories: trees, shrubs and herbs/grasses. With simplifications, these categories can fall respectively in Raunkiær's classes: *Phanerophytae*, *Chamaephyte* and (*Hemi-*) *Cryptophytes* [Raunkiær *et al.*, 1937]. A simplified graphic representation of Raunkiær's life form classification is:

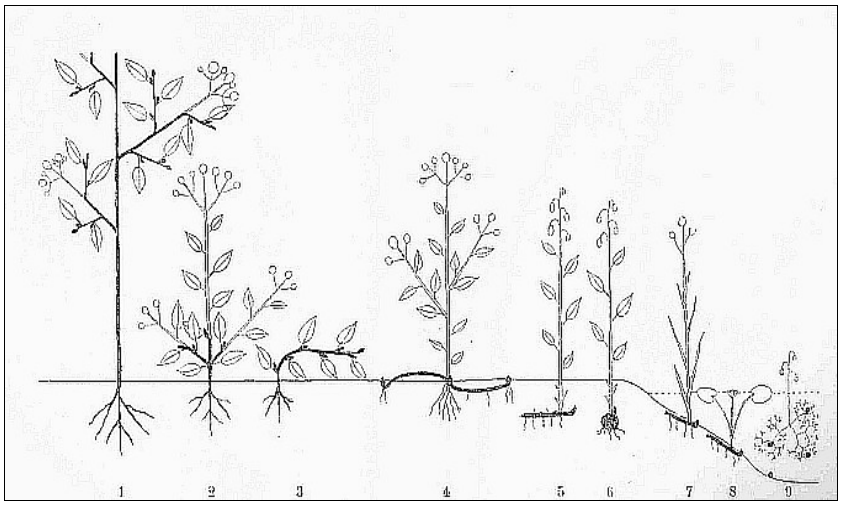

where:

1. *Phanerophyte*
2-3. *Chamaephyte*
4. *Hemicryptophyte*
5-9. *Cryptophyte*

The underling assumption behind Raukiær's life form distinction is the position of the buds in the plant during the resting season (highlighted in the drawing).

Banana trees and plantains can be considered a *Herbaceous* subgroup of *Phanerophyte*. For this and other subdivisions see Ellenberg *et al.* [1967].

10.3 Appendix C

Digitizing sampling polygons, update shape / LUC values and link digital photos with eVis plugin in QuantumGIS

(a) *Create a vector file*

- Start QuantumGIS.
- Load your remote sensed image(s) (e.g. the MASTER subset and the GeoEye-1 mosaic) by clicking on the **Open Raster Layer** icon 
- If you wish to change the image color composite right click on the name in the left list and choose: **Properties → Style** and modify the RGB bands (e.g. for MASTER you can choose the true color composite RGB: 5-3-1). Tick **Use Standard Deviation** and select 2 as factor. Under Contrast enhancement → Current select: **Stretch To MinMax**.
- Click **OK**.
- In case of systematic sampling, load the grid vector file or create it by clicking on the main menu bar **Vector → Research tools → Vector grid.** Select randomly one quadrant by clicking: **Vector → Research tools → Random selection** and select the other grid cells accordingly. Save the so created selected grid cell vector file.
- From the main menu bar: **Layer → New → New Shapefile Layer...** .
- In the New Vector Layer window: tick **Polygon**, specify the Coordinate Reference System (CRS) by browsing to the appropriate set and add a new attribute named for example LUC Class, type Whole number, width e.g. 10. You can also remove the default ID attribute present in the list.
- Click **OK**.
- Save the vector layer (5 files) where preferred.

(b) *Digitize polygons*

- Click on **Settings → Snapping options...** .
- Tick the newly created, the cell grid vector layers, the field Enable topological editing and all the vector layers whose polygons you do not want to overlap (Avoid Overlapping).
- Click **OK**.
- Highlight the vector layer name in the left list if not already highlighted.
- Click on the **Toggle editing** icon on the main menu bar 

- Zoom in to the area you want to digitize. You may help LUC interpretation by overlapping a higher resolution image (e.g. the GeoEye-1 mosaic).
- Once you are sure which pixels to include in the sampling polygon, click on the **Capture polygon** icon.
- Start drawing the verteces of your target polygon by left clicking on the image.
- Terminate digitizing and close the polygon shape by right clicking.
- Type in the LUC class value correspondent to your legend.
- You can continue in this way to digitize the other polygons. To facilitate drawing: play with the Snapping options **Mode** and **Tolerance** values.
- Every once in a while click again on the **Toggle editing** icon to save your work.
- Once you have digitized all target polygons you can separate them in different vector files according to the LUC class by opening the Attribute Table and select the polygons with the same attribute field.

Note: when a pixel cluster lays inside another land use cluster (e.g. a building in the middle of a forest), draw the larger polygon *around* the smaller one. It is important in fact to maintain active the option 'Avoid overlapping' the vector layers in order to avoid pixel miscounting.

(c) *Update polygon shape / LUC value*

- Start a new Quantum GIS project.
- Open the SHP file with the quadrants and the digitized land cover polygons.
- Go to *File → Save as...* and type in a new file name. In this way you **create a copy of the original SHP file** without altering the latter.
- Modify the shape of the wrong polygon(s) using the **Move feature(s)** and **Node tool** from the main menu bar. If interested, annotate of the number of changes.
- Modify the LUC by adding a column to the attribute table and insert the correct value (the Toggle editing mode should be active).
- Remember to save your work regularly.

(d) *Upload GPS points into vector file*

- Connect the GPS receiver to the computer.
- Open DNR Garmin.
- Click *File → Load from → File...*
- Browse to the .GPX file with the recorded waypoints: make sure that the file extension is set to .GPX.

- Select the file and click *Open*.
- As *Feature Type* chose *Waypoint*.
- The waypoints and their associated metadata are uploaded in the *Data Table*.
- To save the data chose *File → Save To → File...* and select the desired folder path. Here you can also chose the file extension (e.g. .SHP, .KML etc.).

(e) *Link digital photos to GPS points in vector file*

- Open both vector layers with the digitized land cover polygons and with the recorded waypoints in Quantum GIS.
- Open the Attribute Table of the waypoint layer.
- Click on **Toggle editing mode** and then on **New column**.
- Name the new column for example 'picture'. Type: **Text**. Width: e.g. 30.
- Click again on **New column** and name it 'height'. Type: **Whole number**. Width: 3.
- Click again on **New column** and name it 'compass'. Type: **Whole number**. Width: 3.
- For each GPS point type in the relative path and picture number (e.g. \pictures\1937.jpg) under the column 'picture'.
- In the column 'height' you can type in the camera height and in 'compass' the bearing.
- Close the **Toggle editing mode** and save your changes.
- Make sure that the layer with the GPS waypoints is selected in the legend window.
- Click on **Plugins → eVis → eVis Event ID tool**.
- *Click on one of the waypoints displayed on the map.*
- In the tab **Options: Attribute containing path to file** → chose **picture**. Tick also **Path is relative** and **Remember this**.
- In the same tab: **Compass bearing → compass.** Tick **Display compass bearing**.
- In the same tab: **Base path** → chose the full path where you saved your pictures. Tick **Remember this**.
- Click **Save**.
- Now by clicking with the eVis Event ID tool on each GPS point that has an associated picture should display the photo.
- Save the project and all layers used. Especially when sharing the document, remember that all files (pictures, vector layers associated files like .SHP, .SHX, .QPJ, .PRJ, .DBF etc.) must be located in the same folder.

10.4 Appendix D

Field form

QUADRANT _____

Date:_____ Sequence number: _____

PICTURES

Polygon ID _____

GPS point: _____ Pic. No.: _____

Direction (º):_____ Camera height (cm):_____

Notes:_____

_____

Polygon ID _____

GPS point: _____ Pic. No.: _____

Direction (º):_____ Camera height (cm):_____

Notes:_____

_____

Polygon ID _____

GPS point: _____ Pic. No.: _____

Direction (º):_____ Camera height (cm):_____

Notes:_____

_____

...

(add an appropriate number of similar sections to survey all polygons)

10.5 Appendix E

Georeferencing and subsetting MASTER-1B products

The following is an adjusted version of the *ENVI© tutorial: Geo-referencing images using Input Geometry* [ENVI© Tutorial: Georeferencing] to suit the specific case of MASTER-1B images.

Required files: MASTER-1B product (*.HDF file);
vector file with study area to be subset.
Required softwares: ITT-ENVI.

(a) - Start ENVI.
- Click on **File → Open External File → Thermal → MASTER**.
- Browse to the MASTER-1B .hdf file.
- On the main menu bar click on **Basic Tools → Resize Data (Spectral/Spatial)**.
- Click on the loaded MASTER data set which appears in the list of Select Input File.
- In Spectral Subset highlight the non-thermal bands (1-25).
- Click OK.
- In the Resize Data Parameters window maintain the default values and set Output to Memory (if the output exceeds the available memory save to File).

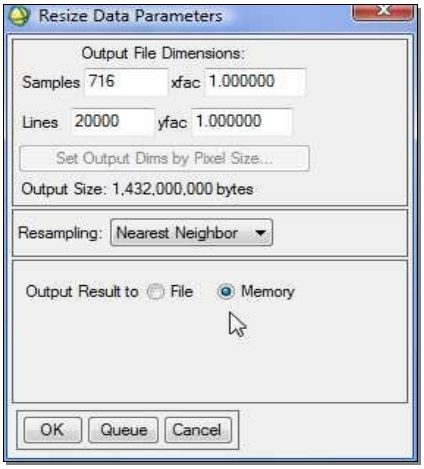

(b) - On the main menu bar click on **File → Open External File → Generic Formats → HDF**.
- Select the same MASTER-1B product and click OK.
- In the HDF Dataset Selection highlight the PixelLatitude and PixelLongitude datasets.

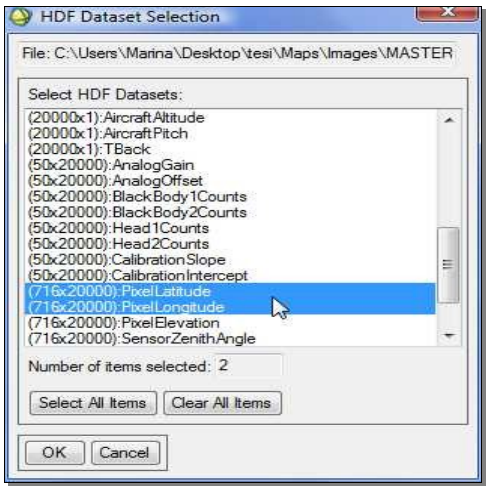

- Click OK.

(c) - On the main menu bar click on **Map → Geometry from Input Geometry → Super Georeference from IGM**[28] .

- As input file select: Memory 1 (the calibrated non-thermal bands).
- Click OK.
- Select as Input X Geometry Band: PixelLongitude and click OK.
- Select as Input Y Geometry Band: PixelLatitude and click OK.
- Select as Input Projection: Geographic Lat/Lon; as Datum: WGS-84; as Units: Degrees; as output Projection: UTM; as Datum: WGS-84; as Units: Meters; as Zone: 17 N.

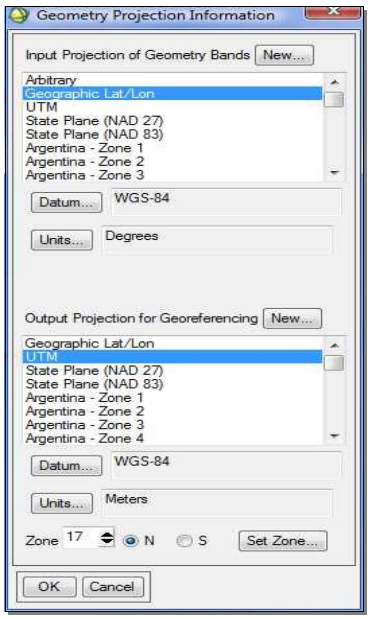

28 IGM: Input GeoMetry

- Click OK

(d) A Build Geometry Lookup File Parameters window opens automatically.

- As Output Pixel Size round the default value (e.g. 9.6 → 10 m).
- As Output Rotation choose 0.
- Accept the other default values.
- Enter an Output SGL[29] file name.
- Save to File the Georef Output and name it.

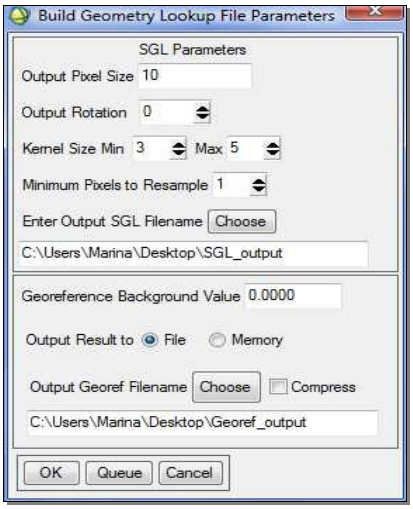

- Click OK.

(e) To sub-set the study area over the georeferenced scene you first need to overlay the vector file:

- In the Available Band List right click on the Georeferenced image and choose **Load True Color**.
- In the Display Image window menu bar select **Overlay → Vectors...**
- In the Vector Parameters: Cursor Query window click on **File → Open Vector File...**
- In the Select Vector Filenames window browse to the vector file defining the study site. Make sure that the search file type is on *.shp if you saved your vector file in such format.
- Select the file and click OK.
- In the Import Vector Files Parameters window evaluate the Native File Projection Parameters and click OK when you are satisfied.
- Visually evaluate the overlaying vector file of the study area.

29 SGL: Super Geometry Lookup table.

(f) Scene subsetting:

- In the Vector Parameter window click on **File → Export Active Layer to ROI**[30]**...**
- In the Export EVF Layers to ROI window choose Convert all records of an EVF layer to one ROI and click OK.
- In the Spatial Subset via ROI Action window select the geoeferenced image produced in (d).
- In the Spatial Subset via ROI Parameters window select the ROI file name corresponding to the study area vector file.
- Select Mask Pixels Outside ROI.
- Enter the Subset Output file name and click OK.

30 ROI: Region Of Interest.

10.6 Appendix F

Atmospherically correct MASTER image with FLAASH-ENVI Module

To perform similar processing with other images or as reference material the interested reader is recommended to consult also the *Atmospheric Correction Module: QUAC and FLAAS User's gui* [ITT-ENVI© Atmospheric Correction Module].

(a) Before running the FLAASH Module you need to create a Filter Function file:

- Go to the MODIS Airborne Simulator webpage, were the MASTER channels are defined (http://mas.arc.nasa.gov/data/srf_html/TC4_master_srf.html).

- Towards the end of the page click on 'Download the SRFs for all bands (*.zip)' and save the folder.

- Unzip the files. The resulting folder contains a list of *.c## files.

- Right click on the first *.c## file on the list (named *msr0807a.c01*) and choose **Open with... .**

- Browse to OpenOffice Calc program and click OK.

- A Text window pops up automatically: make sure that the field 'Space' is ticked.

- Click OK.

- Copy and paste the column with the wavelengths values into a new OpenOffice Calc document. Make sure that in both the original and new document the cell format is set to contain at least 5 significant digits (to change it go to Format → Cells... → Numbers tab).

- Copy and paste the column with the radiance values from the original file to the new Calc document. Make sure that transmittance response values are matched with the corresponding wavelength. Correct the number of significant digits to 6.

- Repeat the previous 2 steps for each band. The result is a Calc document containing a column with wavelength values from 0.4 to 2.55 µm and 25 adjacent columns (one for each band) containing the associated transmittance response.

- Add a 0 in all blank cells. The results looks similar to:

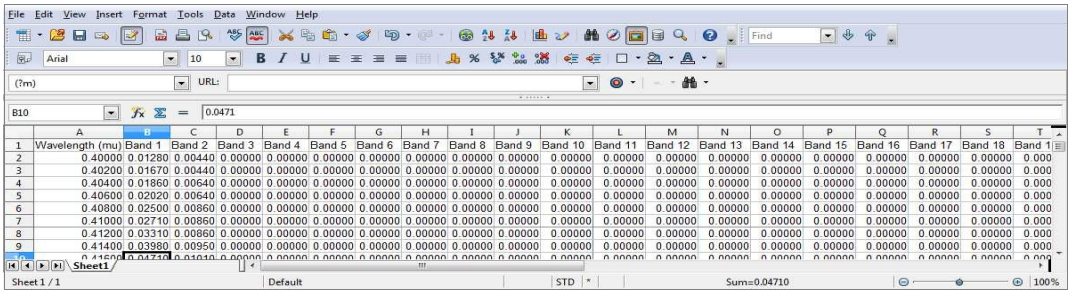

- Save the document both in *.ods format and as ASCII file (e.g. *.txt).
- Start ENVI.
- Go to **Spectral → Spectral Libraries → Spectral Library Builder**.
- Choose **ASCII file** as Input Spectral Wavelength and click OK.
- Browse to the filter function file saved in *.txt.
- An Input ASCII File window opens automatically. Make sure that the wavelength column number is correct (e.g. 1 if you placed it in the first column). You can leave the FWHM column blank. Set Micrometers as Wavelength Unit. Leave 1 as Y Scale Factor.
- Click OK.
- In the Spectral Library Builder window click **Import → From ASCII file...**
- Browse to the same *.txt filter function file and click **Open**.
- In the Input ASCII File window make sure that all 25 Bands are selected in the Select Y Axis Columns. Set the Wavelength Units to Micrometers.
- Click OK.
- In the Spectral Library Builder window now all 25 bands should appear. Click on **Select all** and then **Plot** to view a graph of the transmittance responses of the different bands.
- Save the plot as Image. Save the filer function as Spectral Library file (*.sli).

(b) Run FLAASH Model:

- Open ENVI if you haven't done yet so.
- Go to **Spectral → FLAASH**.
- In the FLAASH Atmospheric correction Model Input Parameters window:

Select as Input Radiance Image the MASTER georeferenced and subset image. In the Radiance Scale Factor windows that opens type in 10.0 as single scale factor for all bands (this is because of the scale conversion from $W/(\mu m \times sr \times m^{2)}$ to $\mu W/(nm \times sr \times cm^2)$).

Choose a name for the Output Reflectance File.

Choose an Output Directory for FLAASH Files.

Choose a Rootname for FLAASH Files (e.g. flaash_).

- In the same window convert the Scene Center Location to DD and type:

Lat 9.89692700
Lon -83.68173500
Sensor Type: UNKNOWN-MSI
Sensor Altitude: 8.457 Km
Ground Elevation: 0.770 Km
Pixel Size: 10 m
Flight Date: March 7th, 2005

Flight Time: 15:16:52 [31]

- As Atmospheric Model choose: Tropical
Water retrieval: No
Water Column Multiplier: 1.00
Aerosol Model: Maritime (see ENVI Atmospheric Correction Module)
Aerosol Retrieval: None
Initial visibility: 40.0 Km

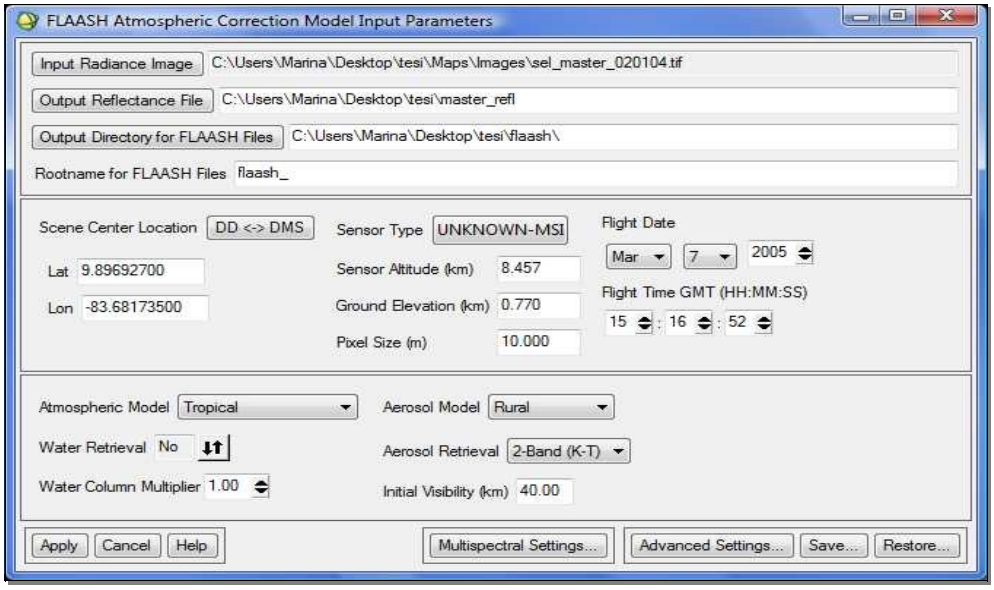

- Then click on the Multispectral button: in the Multispectral Settings window leave GUI as Channel Definer. As Filter Function File browse to the *.sli file.
- Click OK.
- Click Apply.

(c) Scale the values to 2-bytes integer data space.

In (b) you have created an image in reflectance values. You might notice that the reflectance unit in the Z-Spectrum is above 1 (the ratio value you would normally expect is between 0 and 1). This is because it has to be scaled from floating-point to 2-bytes integer data space. Therefore:

- Go to the main ENVI menu bar: **Basic Tools → Band Math.**
- Type in the expression: (b1) / 10000.00.
- Save the new image.

31 These information can be retrieved from the Header file of the original MASTER file (except for the Scene Center that should be calculated in QGIS: Vector → Geometry Tools → Polygon centroid).

10.7 Appendix G

Feature selection in R-Random Forest™ package

Required files: one vector file (e.g. *.shp) for each land use class with all sampling polygons

(a) Export land use ROI to ASCII format readable by R©:

- Start ENVI.
- On the main menu bar: **File → Open Image file** and browse to the MASTER[32] image.
- Click **OK**.
- In the Available Bands List window right click on the image name and choose **Load True Color**.
- In the Image Display window click **Overlay → Vectors...** .
- In the Vector Parameters: Cursor Query window click on **File → Open vector file...** and browse to the vector files with the land use polygons. Remember to set the file extension to the appropriate format in the search menu (e.g. *.shp).
- An Import Vector File window opens. This is because to read *.shp format files ENVI needs to convert them first into *.evf. Check the default parameters and fill in the blank fields.
- Click **OK**.
- In the Vector Parameters: Cursor Query window highlight the first click layer name on the list and then on **File → Export Active Layer to ROI...** .
- In the Export EVF Layers to ROI window choose **Convert all records of an EVF layer to one ROI...** .
- Repeat the previous two steps for all the vector layers.
- Once completed, go to the Image Display menu bar and click **Overlay → Region of Interest...** .
- In the ROI Tool windows which opens automatically you should see all the vector layers exported as ROI. Adjust the class names and colors to your preference.
- Click on Select All. Then on the menu bar **File → Save ROIs... → Select All Items** and choose a suitable name and path. Click **OK**.
- With the files still selected click on **File → Output ROIs to ASCII...** .
- In the Select Input File for ROI data highlight the MASTER image file name. Make

32 You can use both the raw and the atmospherically corrected MASTER image.

sure that all 25 bands are selected in the Spectral subset and then click **OK**.
- In the Output ROIs to ASCII Parameters window select the first item form the list and choose a suitable name and path to save the *.txt file.
- Click on **Edit Output ASCII Form...** .
- In the windows that opens untick 'Geo Location'. Increase the precision of 'Band Values' to 10. Check the other attributes and precision. When satisfied click **OK**.
- Click **OK** in the Output ROIs to ASCII Parameters window.
- Repeat the last 3 steps for all ROI layers of the list.
- Go to the folder where the new *.txt files has been saved. Copy and paste them.
- Rename the copies with *.csv extension. Accept the pop up window warning for possible changes in the file.
- Open the first *.csv file with OpenOffice Calc. In the Text Import window under the Separator option section tick: **Comma**, **Semicolon**, **Space** and **Merge delimiters**. Have a quick look at the preview at the bottom and click **OK**.
- In the Calc document delete the extra header rows, leaving just one row which should display the titles: 'ID', 'X', 'Y', 'LAT', 'LON', 'B1', 'B2', 'B3', ... 'B22'. Delete also the extra columns and make sure that all values are aligned in the right place.
- Go to **File → Save as...** and tick **Filter options**. You can overwrite the modified document on the original *.csv file if you like.
- Repeat the last 5 steps for all ASCII files.

(b) Prepare the R environment for feature selection:
- Start R.

- Load the Rcmdr package by clicking on the main menu bar **Packages → Install packages...** . Choose **Germany (Goettingen)** as CRAN Mirror. Then scroll down the list until Rcmdr and click **OK**. The Rcmdr window is useful to save the input commands for records and future developments. Alternatively to the Rcmdr interface you can use TINN-R (downloadable for free).
- Load the Random Forest package by clicking on the menu bar **Packages → Load packge...** . Scroll down the list until **randomForest**, select it and click **OK**. To save this step type in the the R-Commander window:

```
> install.packages("randomForest", dependencies=TRUE)
```

- Then type:

```
> library(randomForest)
```

- Assign an internal name to each ASCII file created in (a) by typing:

```
> name <- read.csv("full path and name of the *.csv file",
header=TRUE, sep=",")
e.g.                > class1                <-
read.csv("c:/Users/Marina/Documents/Thesis/MASTER_CSV_classe
s/class 1", header=TRUE, sep=",")
```

- Create an internal new column by typing:

```
> name$column name <- as.factor(land use number)
e.g. > class1$class_key <- as.integer(1)
```

- Make sure you repeat the last step for all classes.

- Combine all these internal files using:

```
> new_name <- rbind(name file1, name file 2, …)
```

- Convert the newly created data frame into a ranked data frame by:

```
> new_name$column name <- as.factor(new_name$column name)
e.g. bind_all$class_key <- as.factor(bind_all$class_key)
```

(c) Create a plot which highlights the band importance in determining the land use class:

```
> set.seed(4543)
```

- Create a random forest:

```
> new_name.rf <- randomForest(column name ~ column1 +
column2 + ..., data=new_name, ntree=1000, keep.forest=FALSE,
importance=TRUE)
e.g.> bind_all.rf <- randomForest(class_key ~ B1 + B2 + B3 +
B4 + B5 + B6 + B7 + B8 + B9 + B10 + B11 + B12 + B13 + B14 +
B15 + B16 + B17 + B18 + B19 + B20 + B21 + B22,
data=bind_all,        ntree=1000,        keep.forest=FALSE,
importance=TRUE)
```

- Display two plots calculated with two different accuracy indices:

```
> varImpPlot(new_name.rf)
e.g. > varImpPlot(bind_all.rf)
```

10.8 Appendix H

Feature selection and SVM with EnMAP Toolbox

EnMAP Toolbox is a software developed by Umbold University of Berlin and DLR for image processing and analysis [Suess *et al.*, 2010; Van den Linden *et al.*, 2010 a&b]. Though the overall executing potentials are limited when compared to ITT-ENVI or ERDAS-IMAGINE, some operations are extensively developed. One example is the Support Vector Machine (SVM) algorithm which in EnMAP Toolbox allows to easily evaluate and modify some SVM parameters. A short description of these parameters is provided along this appendix. However for further details and investigations please refer to the EnMAP Box tutorials and manuals.

Data preparation

Before starting with SVM classification you need to format your remote sensed image and reference areas in a way suitable for automatic parametrization of the SVM. For doing this:

1. Open your image in ENVI[33] and from the main menu bar: **File → Save file as... → ENVI Standard**. In this way two files should appear in the chosen directory. It corresponds to the so called *boa_060722* image of the En-MAP Alpine_foreland tutorials.
2. If you have saved the sampling polygons as ROIs overlay them to the MASTER image opened into the Display window and jump to step 6. Otherwise from ENVI main menu bar choose **File → Open Vector File** and browse to the vector files with sampling polygons. Open all of them and eventually save them in *.evf format if you haven't done so yet.
3. In the Available Vector List window choose **Select All Layers → File → Export Active Layers to ROIs...** . As image file to associate choose the MASTER orthorectified and spatially subset image. In the Export EVF Layers to ROI choose: **Convert all records of an EVF Layer to one ROI...** .
4. In the Available Bands List right click on the MASTER image and choose **Load True Color**.
5. In the main menu bar: **Basic Tools → Region of Interest → ROI Tools**. You can now change

33 Currently En-MAP is able to read files with an ENVI-type header. For more info see the Classification Manual [van der Linden *et al.*, 2010a].

the colors of the classes by right clicking on the color names.

6. From the main menu bar: **Classification → Create Class Image form ROI**. Select the MASTER image. Select all ROIs. Finally choose an appropriate path and file name. This corresponds to the so called *lc* file of the Alpine_foreland En-MAP tutorials.

Feature selection

With the just created image file you can now proceed to feature selection. Please follow chapter 2 of the EnMAP Box Regression Tutorial [Suess *et al.*, 2010]. You will create in this way a spectrally subset and scaled image to use for SVM classification. Band selection is based on mainly visual assessment, therefore not very practical for hyperspectral data without prior knowledge on likely atmospheric and spectral windows.

SVM classification

Generate now reference data for SVM analysis by following the steps in chapter 2 of the Classification tutorial [van der Linden *et al.*, 2010b]. You can play with the sampling methodology for reference pixels (Random, Equalized/ Proportional or Disproportional Stratified random) as well as with the number of pixels to consider. Note and appreciate that the pixels used for validation (testing areas) are different from the training set.

Follow now chapter 3 of the Classification Tutorial to parametrize and execute the SVM algorithm. Chapter 4 will guide through a fast accuracy assessment evaluation. Repeat the steps by changing the parameters if necessary. Once you are satisfied proceed with Chapter 5: Apply SVM model to image.

10.9 Appendix I

Field manual

INTRODUCTION

The purpose of this study is to develop an easy and economical methodology for land use and cover (LUC) classification using remote sensed imagery, with particular focus on identification of banana-coffee agroforestry systems.

The expected outcome of this pilot study is to provide useful background material to a team of scientists working on the mapping of a fungi (*Fusarium oxysporum cubense,* FOC) that is severely affecting one important banana cultivar in Central America. This research plan is part of a larger project named "*Mejorando la producción y mercadeo de bananos en cafetales con árboles de pequeños productores: Utilización de los recursos, salud de los suelos, selección de cultivares y estrategias de mercado*" which runs in Costa Rica, Honduras, Nicaragua and Peru.

Due to time and budget restrictions, the procedures proposed in this manual are minimized to an effective workload. The chapter on SAMPLING DESIGN gives a brief overview on the methodology used for indirect land cover classification and preliminary work. FIELD MESUREMENTS and DATA UPLOADING instead provide a complete description of the work to be carried out in the field and the successive data handling.

SAMPLING DESIGN

This section summarizes the procedure followed to select and pre-classify the land cover type within some sample quadrants inside our area of interest before the actual field sampling.

1) Selection of an area 7 x 7 km around Turrialba, CATIE and San Juan Norte. This area of interest is part of 'Site 1' of the project mapping FOC.
2) Drawing of square grid over the selected area → primary quadrants of 200 x 200 m each.
3) Systematic selection of 36 quadrants (distance between selected quadrants 1200 m). The first quadrant has been chosen randomly by the software, the other 35 accordingly (Fig. 19).
4) Preliminary classification of the land cover within these 36 quadrants. With the help of the underlying GeoEye-1 mosaic and MASTER airborne image, the borders of each LUC polygon are digitized with a suitable software (Appendix C). The result is a SHP vector layer of polygons.

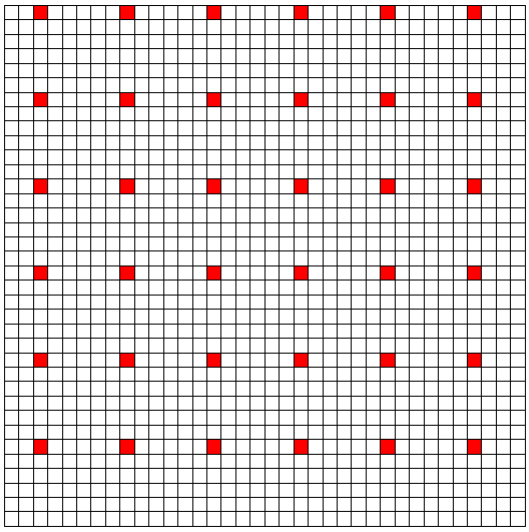

Fig. 19: Grid overlaid to the selected area of 7 x 7 km; each quadrant is 200 x 200 m (real scale). Once the grid was created 36 quadrants were systematically selected (in red). The first quadrant was chosen randomly by the software, the remaining 35 accordingly; this is to ensure an unbiased selection.

5) At the end of each on-screen digitization, a class key number is assigned to the polygons. This number corresponds to one of the land cover classes listed

FIELD MEASUREMENTS

Following there is a complete description of the steps required for the field sampling.

1) Before going to the field, upload some relevant and **easy-to-find GPS points** on a GPS device. These will help identifying the target quadrant in the field. The corresponding waypoint number can be written on the quadrant hard map that you will bring along (you can take a print from the available imagery).
2) Choose one system to **name the quadrants** and therefore facilitate the field work. One idea is to name them with decimal numbers: the whole number before the comma represents the row number, while the decimal number after the comma represents the column number. For example, 6.3 identify the quadrant which lies on the 6th row and on the 3rd column.
3) Go to the field; **navigate the area** and find the selected quadrants with the use of the GPS device and the overview maps (again, remember to take a print with you).
4) Once reached the target quadrant, make a rapid survey to verify that all drawn polygons correspond to the real boundaries. If necessary change the **shape of the polygons** by manually drawing the new version on the quadrant map.

5) **Assign a number to each land cover polygon**. The suggestion is to assign a decimal number, where the whole part corresponds to the class key number and the decimal part to the sequence number. For example, assign the number 5.3 to the 3rd shrub plantation (class key 5) that you encounter in that quadrant. Write the number on the quadrant map with digitized polygons. This will be the record for later land cover data comparison.
6) For all accessible or visible polygons **take a picture**. Use a tripod to maintain the camera in straight position. Automatic camera settings should be used for all photos. Try to capture a good overview of the area you want to photograph but do not alter the camera inclination.
7) Record the **picture number**, **camera height**, **compass bearing** and **GPS point** of the location where the photo is taken from on the field form. Do not forget to write the box and the polygon number on each page. If possible add some notes about the vegetation type, the species and structure. For example: coffee, low Erythrina, tall Laurel.

DATA UPLOADING

At this point, data collected in the field can be transferred to digital format. There are mainly 2 sets of data that need to be uploaded: the land cover information of each polygon and the GPS waypoints with associated pictures. A GIS software such as ArcGIS or Quantum GIS is required to complete this step. See Appendix C for procedure details.

EQUIPMENT

- GPS device (+ reserve batteries)
- compass;
- measurement tape;
- digital camera;
- tripod;
- writing board clip with pencils (+ reserves);
- suitable pens to write on the maps;
- one printed copy of the field sampling chapter;
- one printed copy of the classification key;
- several copies of the field form;
- one printed map of each quadrant with digitized polygons (in scale suitable for writing);
- printed overview maps of the area with the quadrant (in scale suitable for navigating to the target quadrant);
- if possible bring some maps of the area;
- a satellite navigator would obviously help.

11 References

Alavalapati J, Shrestha R, Stainback G, Matta J, 2004. Agroforestry development: An environmental economic perspective. *Agroforestry systems* 61 (1): 299-310.

Arnold G, Fitzgerald M, Grant P, Platnick S, Tsay S, Myers J, King M, Green R, Remer L, 1996. MODIS Airborne Simulator radiometric calibration. Paper presented at the meeting of the Proceedings of SPIE.

ASTER GDEM Validation Team: METI/ERSDAC, NASA/LPDAAC, USGS/EROS, 2009. ASTER Global DEM Validation: Summary report. NASA and METI.

Atkinson P, 1996. Optimal sampling strategies for raster-based geographical information systems. *Global Ecology and Biogeography Letters* 5: 271-280.

Berk A, Bernstein L, Anderson G, Acharya P, Robertson D, Chetwynd J, Adler-Golden S, 1998. MODTRAN cloud and multiple scattering upgrades with application to AVIRIS. *Remote Sensing of Environment* 65 (3): 367-375.

Blomme G, Eden-Green S, Mustaffa M, Nwauzoma B, Thangavelu R, 2011. Major diseases of banana. In *Banana breeding - progress and challenges*, ed. M. Pillay and A. Tenkouano, 85-120. Boca Raton, FL: CRC Press - Taylor & Francis Group.

Breiman L, 2001. Random forests. *Machine learning* 45 (1): 5-32.

Butterfield R and Mariano E, 1995. Screening trial of 14 tropical hardwoods with an emphasis on species native to Costa Rica: fourth year results. *New Forests* 9 (2): 135-145.

Calle M and Urrea V, 2011. Letter to the Editor: Stability of Random Forest importance measures. *Briefings in bioinformatics* 12 (1): 86.

Canty M, 2010. *Image analysis, classification and change detection in remote sensing - With algorithms for ENVI / IDL*. Second ed.: CRC Press - Taylor & Francis Group.

Canty M and Nielsen A, 2008. Automatic radiometric normalization of multitemporal satellite imagery with the iteratively re-weighted MAD transformation. *Remote Sensing of Environment* 112 (3): 1025-1036.

Chang C and Lin C, 2011. LIBSVM: a library for support vector machines. *ACM Transactions on Intelligent Systems and Technology (TIST)* 2 (3): 27.

Chen X, Vierling L, Deering D, 2005. A simple and effective radiometric correction method to improve landscape change detection across sensors and across time. *Remote sensing of environment* 98 (1): 63-79.

Clevers J, Bartholomeus H, Mücher S, De Wit A, 2004. Land cover classification with the medium resolution imaging spectrometer (MERIS). *EARSeL eProceedings* 3 (3): 2004.

Coates A, Jackson J, Collins L, Cronin T, Dowsett H, Bybell L, Jung P, Obando J, 1992. Closure of the Isthmus of Panama: the near-shore marine record of Costa Rica and western Panama. *Geological Society of America Bulletin* 104 (7): 814-828.

Colby J, 1991. Topographic normalization in rugged terrain. *Photogrammetric Engineering and Remote Sensing* 57: 531-537.

Cole R, 2010. Social and environmental impacts of payments for environmental services for agroforestry on small-scale farms in southern Costa Rica. *International Journal of Sustainable Development & World Ecology* 17 (3): 208-216.

Congalton R, 1991. A review of assessing the accuracy of classifications of remotely sensed data. *Remote sensing of environment* 37 (1): 35-46.

Congalton R, 1988. A comparison of sampling schemes used in generating error matrices for assessing the accuracy of maps generated from remotely sensed data. *Photogrammetric engineering and remote sensing (USA)* 54: 593-600.

Congalton R and Green K, 1999. *Assessing the accuracy of remotely sensed data*. CRC Press - Taylor&Francis Group.

Cook OF, 1901. *Shade in coffee culture*. Issue 25 of bulletin. U.S. Dept. of Agriculture, Division of Botany.

Curran P, 1988. The semivariogram in remote sensing: an introduction. *Remote Sensing of Environment* 24 (3): 493-507.

Dahlquist R, Whelan M, Winowiecki L, Polidoro B, Candela S, Harvey C, Wulfhorst J, McDaniel P, Bosque-Pérez N, 2007. Incorporating livelihoods in biodiversity conservation: a case study of cacao agroforestry systems in Talamanca, Costa Rica. *Biodiversity and conservation* 16 (8): 2311-2333.

Di Gregorio A and Jansen LJM, 1998. Land cover classification system (LCCS): classification concepts and user manual. FAO Publications.

Dixon R, 1995. Agroforestry systems: sources of sinks of greenhouse gases? *Agroforestry systems* 31 (2): 99-116.

Efron B and Tibshirani R, 1986. Bootstrap methods for standard errors, confidence intervals, and other measures of statistical accuracy. *Statistical science*: 54-75.

Ellenberg H, Mueller Dombois D, 1967. A key to Raunkiaer plant life forms with revised subdivisions. *Ber. geobot. Inst. eidg. tech. Hochschule Rubel* 37: 56-73.

Erbek S, Ozkan C, Taberner M, 2004. Comparison of maximum likelihood classification method with supervised artificial neural network algorithms for land use activities. *International Journal of Remote Sensing* 25 (9): 1733-1748.

Eurimage, 2011. *Product level: description*. [online] available at <www.eurimage.it/products/products.html > accessed on 15th August 2011.

Eva H, Belward A, De Miranda A, Di Bella C, Gond V, Huber O, Jones S, Sgrenzaroli M, Fritz S, 2004. A land cover map of South America. *Global Change Biology* 10 (5): 731-744.

FAO, 2003. WTO agreement on agriculture: the implementation experience - Developing countries case studies.

FAO, 2006. World Soil Resources World reference base for soil resources. IUSS Working Group WRB (World Reference Base)(103). ISBN 92-5-105511-4.

Fitzpatrick-Lins K, 1981. Comparison of sampling procedures and data analysis for a land-use and land-cover map. *Photogrammetric Engineering and Remote Sensing* 47 (3): 343-351.

Foody G, 2000. Accuracy of thematic maps derived by remote sensing. Paper presented at the meeting of the Proceedings of the accuracy 200 conference, Amsterdam.

Foody G and Mathur A, 2004. Toward intelligent training of supervised image classifications: directing training data acquisition for SVM classification. *Remote Sensing of Environment* 93 (1-2): 107-117.

Foody G, Mathur A, Sanchez-Hernandez C, Boyd D, 2006. Training set size requirements for the classification of a specific class. *Remote Sensing of Environment* 104 (1): 1-14.

FRA, 2000a. Forest cover mapping & monitoring using NOAA-AVHRR & other coarse-resolution sensors. Working Paper 29, FAO Rome.

FRA, 2000b. On definitions of forest and forest change. FAO, Rome.

FRA, 2010. Global forest resources assessment: terms and definitions. Working paper 144/E, FAO Rome.

Franklin S, Wulder M, 2002. Remote sensing methods in medium spatial resolution satellite data land cover classification of large areas. *Progress in Physical Geography* 26 (2): 173.

French A, Schmugge T, Kustas W, 2000. Discrimination of senescent vegetation using thermal emissivity contrast. *Remote sensing of environment* 74 (2): 249-254.

Fuchs HJ, Kleinn C, Zamora S, Aberle H, 2010. BP- TechReport1. AWF Göttingen University. Unpublished technical report.

Gelli G and Poggi G, 1999. Compression of multispectral images by spectral classification and transform coding. *Image Processing, IEEE Transactions on* 8 (4): 476-489.

Gomez C, Mangeas M, Petit M, Corbane C, Hamon P, Hamon S, De Kochko A, Le Pierres D, Poncet V, Despinoy M, 2010. Use of high-resolution satellite imagery in an integrated model to predict the distribution of shade coffee tree hybrid zones. *Remote Sensing of Environment* 114 (11): 2731-2744.

Green A, Berman M, Switzer P, Craig M, 1988. A transformation for ordering multispectral data in terms of image quality with implications for noise removal. *Geoscience and Remote Sensing, IEEE Transactions on* 26 (1): 65-74.

Gretton A, Herbrich R, Chapelle O, Rayner PJW, 2001. Estimating the Leave-One-Out Error for Classification Learning with SVMs. *Citeseer.*

Haklay M and Weber P, 2008. OpenStreetMap: User-generated street maps. *Pervasive Computing, IEEE* 7 (4): 12-18.

Hook S, Myers J, Thome K, Fitzgerald M, Kahle A, 2001. The MODIS/ASTER airborne simulator (MASTER)–a new instrument for earth science studies. *Remote Sensing of Environment* 76 (1): 93-102.

Hsu C and Lin C, 2002. A comparison of methods for multiclass support vector machines. *Neural Networks, IEEE Transactions on* 13 (2): 415-425.

Huang C, Davis L, Townshend J, 2002. An assessment of support vector machines for land cover classification. *International Journal of Remote Sensing* 23 (4): 725-749.

Hubert-Moy L, Cotonnec A, Le Du L, Chardin A, Perez P, 2001. A comparison of parametric classification procedures of remotely sensed data applied on different landscape units. *Remote Sensing of Environment* 75 (2): 174-187.

Hughes G, 1968. On the mean accuracy of statistical pattern recognizers. *Information Theory, IEEE Transactions on* 14 (1): 55-63.

IAAST, 2008. Agriculture at a crossroads: Global report. International Assessment of Agricultural Knowledge, Science and Technology for Development, Washington DC - Island Press.

ICRAF, 1993. Annual report 1993. International Centre for Research in Agroforestry, Nairobi.

Isaac M, 2009. Ecological and social interactions in sustainable agroforestry management: Cocoa in Ghana. PhD diss. University of Toronto.

ISDA, 2011. Project: Large geospacial datasets - Costa Rica 2050. Image Spatial Analysis Group. http://isda.ncsa.uiuc.edu/Costarica

ITT-ENVI Atmospheric Correction Module: QUAC and FLAASH User's guide. http://www.ittvis.com/portals/0/pdfs/envi/Flaash_Module.pdf.

ITT-ENVI ENVI Tutorial: Classification methods. http://www.ittvis.com/portals/0/tutorials/envi/Classification_Methods.pdf.

ITT-ENVI ENVI Tutorial: Georeferncing Images using Input Geometry. http://www.ittvis.com/portals/0/tutorials/envi/Georef_Input_Geometry.pdf.

ITT-ENVI ENVI Tutorial: Mosaicking in ENVI. http://www.ittvis.com/portals/0/tutorials/envi/Mosaicking.pdf.

ITT-ENVI, 2001. *ENVI Tutorials*. Research systems ed, 620 pg.

Jensen JR, 2000. *Remote sensing of the environment - An Earth resource perspective*. Prentice Hall.

Jose S, 2009. Agroforestry for ecosystem services and environmental benefits: an overview. *Agroforestry Systems* 76 (1): 1-10.

Karpouzli E and Malthus T, 2003. The empirical line method for the atmospheric correction of IKONOS imagery. *International Journal of Remote Sensing* 24 (5): 1143-1150.

Kass D, Jimenez M, Kauffman J, Herrera-Reyes C, 1995. Reference soils of the Turrialba valley and slopes of the Irazu volcano. In *Soil Brief Costa Rica*. ISRIC.

Kearns M and Ron D, 1999. Algorithmic stability and sanity-check bounds for leave-one-out cross-validation. *Neural Computation* 11 (6): 1427-1453.

Keuchel J, Naumann S, Heiler M, Siegmund A, 2003. Automatic land cover analysis for Tenerife by supervised classification using remotely sensed data. *Remote Sensing of Environment* 86 (4): 530-541.

Kleinn C, 2007. Lecture notes for the teaching module Forest Inventory. 1st revised ed.

Kottek M, Grieser J, Beck C, Rudolf B, Rubel F, 2006. World Map of the Koppen-Geiger climate classification updated. *Meteorologische Zeitschrift* 15 (3): 259-263.

Kruse F, 2004. Comparison of ATREM, ACORN, and FLAASH atmospheric corrections using low-altitude AVIRIS data of Boulder, CO. Paper presented at the meeting of the 13th JPL Airborne Geoscience Workshop.

Kumar BM, 2006. Carbon sequestration potential of tropical homegardens. In *Kumar BM and Nair PKR: Tropical Homegardens: A Time-Tested Example of Sustainable Agroforestry*, 185–204. Dordrecht, the Netherlands. Springer.

Lagemann J and Heuveldop J, 1983. Characterization and evaluation of agroforestry systems: the case of Acosta-Puriscal, Costa Rica. *Agroforestry systems* 1 (2): 101-115.

Landgrebe D, 1999. Information extraction principles and methods for multispectral and hyperspectral image data. *Information processing for remote sensing* 82: 3-38.

Law K and Nichol J, 2004. Topographic correction for differential illumination effects on IKONOS satellite imagery. *International Archives of Photogrammetry Remote Sensing and Spatial Information*: 641-646.

Li P and Moon W, 2004. Land cover classification using MODIS-ASTER airborne simulator (MASTER) data and NDVI: a case study of the Kochang area, Korea. *Canadian Journal of Remote Sensing* 30 (2): 123-136.

Lichtemberg PdSF, 2010. Occurrence, incidence and grower perception of Fusarium oxysporum f.sp. cubense in banana intercropped with coffee and trees in Costa Rica and Nicaragua smallholders. Masters thesis, Universität Bonn, Germany.

Loveland T, Reed B, Brown J, Ohlen D, Zhu Z, Yang L, Merchant J, 2000. Development of a global land cover characteristics database and IGBP DISCover from 1 km AVHRR data. *International Journal of Remote Sensing* 21 (6/7): 1303-1330.

Lu D, Mausel P, Brondizio E, Moran E, 2002. Assessment of atmospheric correction methods for Landsat TM data applicable to Amazon basin LBA research. *International Journal of Remote Sensing* 23 (13): 2651-2671.

Mahiny A and Turner B, 2007. A comparison of four common atmospheric correction methods. *Photogrammetric engineering and remote sensing* 73 (4): 361.

Malinverni E, Tassetti A, Mancini A, Zingaretti P, Frontoni E, Bernardini A, 2011. Hybrid object-based approach for land use/land cover mapping using high spatial resolution imagery. *International Journal of Geographical Information Science* 25 (6): 1025-1043.

Mather P, 2004. *Computer processing of remotely-sensed images*. Wiley Online Library.

Matthew M, Adler-Golden S, Berk A, Felde G, Anderson G, Gorodetzky D, Paswaters S, Shippert M, 2003. Atmospheric correction of spectral imagery- Evaluation of the FLAASH algorithm with AVIRIS data. Paper presented at the meeting of the Proceedings of SPIE.

McRoberts RE and Meneguzzo DA, 2007. Estimating tree species richness from forest inventory plot data. Notes from the 2005 Proceedings of the Seventh Annual Forest Inventory and Analysis Symposium, 275-279.

Miller R and Nair P 2006. Indigenous agroforestry systems in Amazonia: from prehistory to today. *Agroforestry systems* 66 (2): 151-164.

Montagnini F, 2006. *Homegardens of Mesoamerica: biodiversity, food security, and nutrient management*. Springer.

Mooney P, Corcoran P, Winstanley A, 2010. Towards quality metrics for OpenStreetMap. Paper presented at the meeting of the Proceedings of the 18th SIGSPATIAL International Conference on Advances in Geographic Information Systems.

Nair P, Kumar B, Nair V, 2009. Agroforestry as a strategy for carbon sequestration. *Journal of Plant Nutrition and Soil Science* 172 (1): 10-23.

Nair PKR, 1993. *An introduction to agroforestry*. Klgwer Academic Publishers.

Nair PKR, 1985. Classification of agroforestry systems. *Agroforestry systems* 3 (2): 97-128.

Nair PKR and Nair VD, 2003. Carbon Storage in North American Agroforestry Systems. In *Kimble J, Heath LS, Birdsey RA and Lal R. (eds). The Potential of U.S. Forest Soils to Sequester Carbon and Mitigate the Greenhouse Effect*. Boca Raton, FL: CRC Press LLC.

NASA 2008. MASTER. Jet Propulsion Laboratory. http://masterweb.jpl.nasa.gov/.

NASA, 2005. CARTA, 2005 Final - Flight Summary Report., Airborne sensor facility - NASA Ames Research Center.

Nemani R, Running S, 1997. Land cover characterization using multitemporal red, near-IR, and thermal-IR data from NOAA/AVHRR. *Ecological Applications* 7 (1): 79-90.

Olschewski R, Tscharntke T, Benitez P, Schwarze S, Klein A 2006. Economic evaluation of pollination services comparing coffee landscapes in Ecuador and Indonesia. *Ecology and Society* 11 (1): 7.

Palma J, Graves A, Bunce R, Burgess P, De Filippi R, Keesman K, Van Keulen H, Liagre F, Mayus M, Moreno G, others, 2007. Modeling environmental benefits of silvoarable agroforestry in Europe. *Agriculture, ecosystems & environment* 119 (3-4): 320-334.

Ploetz R and Churchill A, 2009. Fusarium wilt: the banana disease that refuses to go away. Paper presented at the meeting of the Proceedings of International ISHS/ProMusa Banana Symposium.

Ploetz RC, Pehh KG, Jones DR, Stover RH, Lomerio EO, Tessera M, Quimio AJ, 1999. Fungal diseases of the root, corm and pseudostem. In *Disease of banana, abaca and enset*. CABI Publishing.

Plourde L and Congalton R, 2003. Sampling method and sample placement: How do they affect the accuracy of remotely sensed maps? *Photogrammetric engineering and remote sensing* 69 (3): 289-297.

Pocasangre L, Ploetz R, Molina A, Vicente LP, 2011. Raising awareness of the threat of Fusarium wilt tropical race 4 in Latin America and the Carribean. Paper presented at the meeting of the ISHS Acta Horticulturae 897: International ISHS-ProMusa Symposium on Global Perspectives on Asian Challenges.

Pocasangre L and Pérez-Vincente L, 2009. Impacto potencial de la entrada de raza tropical 4 del mal de Panamà (Fusarium oxysporum f.sp. cubense) en la industria bananera y platanera de América Latina y el Caribe. In *Taller de entrenamiento sobre diagnòstico y caracterizaciòn de la marchitez por Fusarium o Mal de Panamà*. Bioversity International.

Raunkiaer C and Gilbert-Carter H, 1937. *Plant life forms*. The Clarendon Press.

Reisner Y, De Filippi R, Herzog F, Palma J, 2007. Target regions for silvoarable agroforestry in Europe. *Ecological engineering* 29 (4): 401-418.

Richards JA and Jia X, 1999. *Remote Sensing Digital Image Analysis: An Introduction*. 3rd Edited by Ricken DE and Gessner W. Secaucus, NJ, USA: Springer-Verlag New York, Inc.

Russo R and Budowski G, 1986. Effect of pollarding frequency on biomass of Erythrina poeppigiana as a coffee shade tree. *Agroforestry systems* 4 (2): 145-162.

Schwarz M and Zimmermann N, 2005. A new GLM-based method for mapping tree cover continuous fields using regional MODIS reflectance data. *Remote Sensing of Environment* 95 (4): 428-443.

Smith GM and Milton EJ, 1999. The use of the empirical line method to calibrate remotely sensed data to reflectance. *International Journal of Remote Sensing* 20 (13): 2653-2662.

Stehman S, 1992. Comparison of systematic and random sampling for estimating the accuracy of maps generated from remotely sensed data. *Photogrammetric Engineering and Remote Sensing* 58 (9): 1343-1350.

Stehman S and Czaplewski R, 1998. Design and Analysis for Thematic Map Accuracy Assessment: Fundamental Principles. *Remote Sensing of Environment* 64 (3): 331-344.

Strahler A, 1980. The use of prior probabilities in maximum likelihood classification of remotely sensed data. *Remote Sensing of Environment* 10 (2): 135-163.

Suess S, van der Linden S, Leitão PJ, Rabe A, Wirth F, Okujeni A, Hostert P, 2010. En-MAP Box Tutorial: SVM regression. Humboldt-Universität zu Berlin, Germany.

Thacher T, Lee D, Schelhas J, 1996. Farmer participation in reforestation incentive programs in Costa Rica. *Agroforestry Systems* 35 (3): 269-289.

Thomlinson J, Bolstad P, Cohen W, 1999. Coordinating methodologies for scaling landcover classifications from site-specific to global: Steps toward validating global map products. *Remote Sensing of Environment* 70 (1): 16-28.

Tornquist C, Hons FM, Feagley SE, Haggar J, 1999. Agroforestry system effects on soil characteristics of the Sarapiqui region of Costa Rica. *Agriculture, ecosystems & environment* 73 (1): 19-28.

Tso B and Mather P, 2009. *Classification methods for remotely sensed data*. Second Boca Raton, FL: CRC Press - Taylor & Francis Group.

Unruh J and Lefebvre P, 1995. A spatial database approach for estimating areas suitable for agroforestry in subSaharan Africa: aggregation and use of agroforestry case studies. *Agroforestry systems* 32 (1): 81-96.

Van Asten P, Wairegi L, Mukasa D, Uringi N, 2011. Agronomic and economic benefits of coffee-banana intercropping in Uganda's smallholder farming systems. *Agricultural Systems* 104 (4): 326-334.

Van der Linden S, Rabe A, Wirth F, Suess S, Okujeni A, Hostert P, 2010a. imageSVM Classification Manual for Application: imageSVM (2.1). Humboldt-Universität zu Berlin, Germany.

Van der Linden S, Wirth F, Leitão P, Rabe A, Suess S, Okujeni A, Hostert P, 2010b. En-MAP Box Application Tutorial: SVM Classification. Humboldt-Universität zu Berlin, Germany.

Van der Meer F, 1999. Geostatistical approaches for image classification and assessment of uncertainty in geologic processing. In *Advances in remote sensing and GIS analysis*, ed. P. Atkinson and N. Tate, 147-166. Chichester: John Wiley and Sons.

Van Genderen J, Lock B, Vass P, 1978. Remote sensing: statistical testing of thematic map accuracy. *Remote Sensing of Environment* 7 (1): 3-14.

Vermote E, Tanré D, Deuze J, Herman M, Morcette J, 1997. Second simulation of the satellite signal in the solar spectrum, 6S: An overview. *Geoscience and Remote Sensing, IEEE Transactions on* 35 (3): 675-686.

Walter V, 2004. Object-based classification of remote sensing data for change detection. *ISPRS Journal of Photogrammetry and Remote Sensing* 58 (3-4): 22--238.

Wang G, Gertner G, Anderson A, 2005. Sampling design and uncertainty based on spatial variability of spectral variables for mapping vegetation cover. *International Journal of Remote Sensing* 26 (15): 3255-3274.

Whitley E and Ball J, 2002. Statistics review 6: Nonparametric methods. *Critical care* London 6(6): 509-513.

Woodcock C, Strahler A, Jupp D, 1988. The use of variograms in remote sensing: II. Real digital images. *Remote Sensing of Environment* 25 (3): 349-379.

Xie Y, Sha Z, Yu M, 2008. Remote sensing imagery in vegetation mapping: a review. *Journal of Plant Ecology* 1 (1): 9.

Yu Q, Gong P, Clinton N, Biging G, Kelly M, Schirokauer D, 2006. Object-based detailed vegetation classification with airborne high spatial resolution remote sensing imagery. *Photogrammetric Engineering and Remote Sensing* 72 (7): 799.

Zomer RJ, Tabucco A, Coe R, Place F, 2009. Trees on farm: analysis of global extend and geographical patterns of agroforestry. ICRAF - working paper no.89, World Agroforestry Centre, Nairobi, Kenya.

Declaration of authorship

Hiermit versichere ich gemäß § 9 Abs. 5 der Master-Prüfungsordung vom 22.07.2005, dass ich die vorliegende Arbeit selbständig verfasst und keine anderen als die angegebenen Quellen und Hilfsmittel benutzt habe.

22/September/2011

Marina Martignoni